Validation of Ozone Monitoring Instrument Nitrogen Dioxide Columns

E. A. Celarier,[1] E. J. Brinksma,[2] J. F. Gleason,[3] J. P. Veefkind,[2] A. Cede,[4]

J. R. Herman,[3] D. Ionov,[5,6] F. Goutail,[6] J-P. Pommereau,[6] J-C. Lambert,[7]

M. van Roozendael,[7] G. Pinardi,[7] F. Wittrock,[11] A. Schönhardt,[11]

A. Richter,[11] O. W. Ibrahim,[13] T. Wagner,[12] B. Bojkov,[4] G. Mount,[8]

E. Spinei,[8] C. M. Chen,[9] T. J. Pongetti,[9] S. P. Sander,[9] E. J. Bucsela,[4]

M. O. Wenig,[4] D. P. J. Swart,[10] H. Volten,[2,10] M. Kroon,[2] and P. F. Levelt[2]

Edward A. Celarier, SGT, Inc. 7701 Greenbelt Rd, Greenbelt, MD 20770 (Edward.Celarier@gsfc.nasa.gov)

Ellen Brinksma, KNMI, 3730 AE De Bilt, The Netherlands (ellen.brinksma@knmi.nl)

[1] SGT, Inc., 7701 Greenbelt Rd Ste 400,

Abstract. We review the standard nitrogen dioxide (NO_2) data product (Version 1.0.0), which is based on measurements made in the spectral region 415–465 nm by the Ozone Monitoring Instrument (OMI) on the EOS-Aura satellite. A number of ground- and aircraft-based measurements have been used to validate the data product's three principal quantities: stratospheric, tropospheric, and total NO_2 column densities. It is found that OMI underestimates the stratospheric column by about 14%, and underestimates both the total and tropospheric columns by $15 - 30\%$. The validation of the OMI NO_2 data is complicated by the fact that some of the ground based measurements have not been well validated, themselves, and by problems inherent in comparing point measurements from the ground to large area averaged satellite measurements. In addition, some of the ground based measurements have only been made over a relatively short period of time, limiting their use for statistical comparison with OMI. Nonetheless, by using all the available ground based measurements, it is possible to arrive at some quantitative characterization of the biases in the OMI NO_2 data product.

Greenbelt MD 20770, USA.

1. Introduction

The Ozone Monitoring Instrument (OMI) is a space borne spectroradiometer that uses a 2-dimensional CCD array detector to simultaneously measure the spectra of the earth shine radiance at large number of viewing angles, approximately transverse to the Aura spacecraft's flight track. OMI measures in three broad spectral regions (UV-1, UV-2, and VIS), with a spectral resolution on the order of 0.5 nm. Applying spectral fitting techniques to the OMI data permits the simultaneous retrieval of a wide range of atmospheric trace gas concentrations as well as cloud and aerosol properties and loadings. Among the trace gases that can be retrieved, ozone (O_3) and nitrogen dioxide are identified as essential measurements, both for the ongoing monitoring of the Earth's stratospheric ozone layer and for the monitoring of tropospheric air quality. A more extensive discussion of the OMI instrument itself can be found in *Levelt and Bhartia* [2007].

The OMI NO_2 data production algorithm is designed to retrieve total vertical column densities of NO_2 and separate stratospheric and tropospheric column densities; this enables the improvement in the calculation of the total vertical column. This separation is important (and possible) because the chemistry and dynamics of NO_2 are different between the stratosphere and the troposphere. Accurate measurements of the tropospheric NO_2 are significant for the characterization of air quality, a primary objective of the Aura and OMI missions.

This paper discusses only the validation of the OMI NO_2 standard product, archived at the Goddard Earth Sciences Data and Information Services Center (GES-DISC). We do not

---

[2] Royal Netherlands Meteorological

discuss any other product, such as the Level-4 product, archived at the Royal Netherlands Meteorological Institute (KNMI). Furthermore, comparison of OMI to other spaceborne NO_2 sensors, which all have different equator crossing times from OMI is beyond the scope of this paper.

A number of efforts toward NO_2 validation have been initiated, in which measurements are made coincident with OMI overpass measurements. The purpose of this paper is to provide an overview of results from these efforts. A variety of instruments and techniques have been used, each with its characteristic sensitivity to stratospheric, tropospheric, or total column NO_2. This paper will address the advantages and, in some cases, the limitations of the various measurements.

Several of the techniques described are new, and have not been well-validated. In addition, there is an essential difference between observations of NO_2 taken from the ground, and observations averaged over a satellite field of view (FOV). Spatial inhomogeneity, characteristic of airborne constituents emitted at (possibly moving) point sources, and subject to surface-level winds, implies that a single point measurement will often not be a representative sample within a "collocated" satellite FOV covering a region of the order of several hundred square kilometers. Monthly average comparisons of ground-based and satellite measurements can remove much of the variability due to FOV-point measurement differences. A preliminary measurement of horizontal inhomogeneity in the NO_2 field is presented in the DANDELIONS overview paper [*Brinksma et al.*, 2007], using a set of simultaneous tropospheric NO_2 measurements made at different azimuths. *Veefkind et al.* [2007] show a comparison of regridded OMI NO_2 data with ground-based observations by

---

Institute, 3730 AE De Bilt, The

the Dutch national air quality network. This network distinguishes regional stations, and city and street stations, which are close to source regions. For the period of the satellite data, NO_2 reported by 35 stations around the Netherlands, averaged between 11:00 and 14:00 h local time, was compared to the collocated OMI measurements. A strong correlation ($R = 0.94$) between the satellite data and the regional station data was found. By contrast, correlations with urban stations are weak, because local conditions may vary strongly over a few hundred meters, far smaller than the spatial resolution of OMI. Because of both the novelty of some of the techniques, and such spatial-scale effects, specific results are sometimes limited to qualitative, or order-of-magnitude, conclusions.

Among the validation studies discussed here are ground based observations made within the SAOZ and DOAS networks. These are zenith-sky, twilight measurements, which are sensitive to the stratospheric NO_2 column (as explained in section 4.1.1). In addition, the locations are very often pristine areas, or at elevation. Even if the instrumentation were sensitive to tropospheric NO_2, the lack of pollution would lead to measurements dominated by the stratospheric NO_2 amount.

To focus on polluted areas, where satellite NO_2 retrievals are most challenging, novel, or as yet unvalidated techniques must be used.

Measurements of scattered light by the MultiAxial DOAS (MAX-DOAS) technique [*Platt*, 1994; *Wittrock et al.*, 2004], using a range of viewing angles, from nearly horizontal through zenith, are sensitive to the tropospheric part of the column, and provide both total and

---

Netherlands.

tropospheric NO_2 amounts. We present results from MAX-DOAS measurements taken in a polluted area, but away from immediate local sources, in section 4.2.1.

Direct-sun ground based measurements, made with a Brewer spectrophotometer [*Cede et al.*, 2006] and with newly-developed direct-sun instruments, including a high-resolution Fourier-transform UV-FTS technique [*Cageao et al.*, 2001], and a number of direct-sun DOAS-type measurements, are sensitive to the total NO_2 column. We will briefly review some preliminary results from these methods in section 4.3.

Validation of the OMI NO_2 data should take account of the sensitivity of the numerous geophysical and geometric algorithmic inputs. These include the *a priori* profile shapes, surface albedo, and measured and assumed cloud properties. These, in particular, greatly affect the air mass factors (AMF; the ratio of slant-column density of the absorber along the optical path to the vertical column density) the algorithm calculates. Tropospheric NO_2 profiles have been measured with lidar in the Netherlands, during a number of days in September 2006, and with airborne instrumentation during various validation campaigns.

During the Polar Aura Validation Experiment (PAVE) (flights from New Hampshire, January and February 2005) the TD-LIF instrument [*Thornton et al.*, 2000; *Cleary et al.*, 2002] was used for *in situ* sampling of NO_2, during the aircraft flights. The NASA DC-8 performed two flight legs at 300 m altitude, near the top of the boundary layer. When flights entered the boundary layer, strongly enhanced concentrations of NO_2 were found.

During the INTEX-B campaign (flights from Houston, Texas, March 2006 and from Honolulu, Hawaii, and Anchorage, Alaska, April and May 2006) the TD-LIF instrument

---

[3] Code 613.3, NASA Goddard Space

measured NO_2 *in situ*. Spirals were flown by the NASA DC-8 during several flights in spatial and temporal collocation with OMI observations.

Besides INTEX-B, a small number of other airborne campaigns have been carried out, measuring NO_2 *in situ*, and have been applied to satellite validation [*Heland et al.*, 2002; *Martin et al.*, 2006].

The remainder of Section 1 contains a brief description of NO_2 chemistry in the stratosphere and troposphere, the OMI measurement of NO_2, and the availability of the data sets. Section 2 describes the OMI measurement, and Section 3 describes the algorithm that reduces the raw OMI measurements to the various NO_2 columns. The various subsections of Section 4 discuss the validations of the three principal NO_2 products: stratospheric column (Section 4.1), tropospheric column (Section 4.2), and total column (Section 4.3). The conclusions are presented in Section 5.

1.1. Nitrogen dioxide in the stratosphere

Nitrogen dioxide participates both directly and indirectly in the catalytic destruction of ozone in the stratosphere [*Finlayson-Pitts and Pitts*, 2000]. Direct catalytic destruction takes place via a $NO - NO_2$ cycle that catalyzes the reaction $O_3 + O \rightarrow 2O_2$, while while NO_2 concentrations indirectly control ozone loss through other catalytic cycles by controlling, for example, the distribution of chlorine between its catalytically active (ClO) and inactive, reservoir ($ClONO_2$) species. In the stratosphere, NO_2 concentration has a distinctive diurnal cycle, due largely to the photochemistry of nitrogen oxides. At night, all the photolysis reactions stop, shifting the steady state to NO_2. NO_2 is converted,

---

Flight Center, Greenbelt MD 20771, USA.

through ozonolysis, to NO_3, which can further combine with NO_2 to form N_2O_5. This results in a slow decrease of NO_2 over the course of the night. When the air is again sunlit, the N_2O_5 rapidly redissociates to NO_2 and NO_3, which photolyzes instantaneously, mostly to NO. Meanwhile, NO_2 photolyzes very rapidly, and so decreases very rapidly at sunrise. While in daylight, the dominant processes are the interconversion between NO and NO_2. Under most typical conditions of temperature and ozone concentration, latitude, and season, there is a slow increase in NO_2 concentration over the course of the daylight hours. In addition to the chemical and photochemical processes, transport by the winds, particularly in the vicinity of the polar jets may mean that the air that one is measuring has not had the photochemical history one would expect, based on location and local time, alone. Some caution is therefore needed in matching satellite measurements to the ground based measurements.

1.2. Nitrogen dioxide in the troposphere

In the troposphere, nitrogen oxides are a significant contributor to poor air quality. Gaseous NO_2 is red in color, and gives rise to the characteristic brownish cast of polluted air. Both NO and NO_2 are harmful to lung tissue, and, as a powerful oxidizing agent, NO_2 is harmful to biological tissue generally. Besides its direct effects, photolysis of NO_2 contributes to ozone production [*Finlayson-Pitts and Pitts*, 2000] according to

$$\begin{aligned} \mathrm{NO_2 + h\nu} &\longrightarrow \mathrm{NO + O} \\ \mathrm{O + O_2} &\longrightarrow \mathrm{O_3} \end{aligned}$$

---

[4] GEST Program, University of Maryland

Nitrogen oxides are produced in high-temperature processes, most notably in combustion (fossil fuels and biomass burning) and in lightning. As a rule, the higher the combustion temperature, the more NOx is produced. Nearly all the NOx ($NO + NO_2$) that is significant for human health is produced by industrial and urban activity, including transportation and power generation.

NO_2 is removed from the troposphere through conversion to HNO_3, nitric acid, which readily dissolves in any available water droplets. NO_2 plumes are detected only up to about 200 km from their source. In the neighborhood of industrial or urban sources, there is a distinct diurnal pattern in the concentration of NOx. The diurnal signal at any location is the result of a complex interplay between the emission source field in space and time, photochemical lifetimes, advection, and the concentrations of chemical sinks for NOx species. As mentioned before, these also give rise to spatial inhomogeneities on a sub-100 m scale. At mid- to low-latitudes, where a polar-orbiting satellite passes over a given location is only once or twice a day, the satellite only sees a “snapshot” of the state of the polluted atmosphere at the overpass times. In the mid-to-upper latitudes, inconsistent measurements, from one orbit to the next, over some location, may well result from significant changes in the NO_2 concentrations over the intervening 100 minutes, as well as from other rapid geophysical changes, e.g. in cloud cover.

1.3. OMI measurement of NO_2

The Aura satellite is a polar-orbiting, sun-synchronous satellite, whose orbital period is 99 minutes. Aura flies over the entire surface of the Earth every 14–15 orbits. Using

---

Baltimore County, Baltimore MD, USA.

the 2-dimensional CCD array detector, with pixel binning factors chosen to optimize the signal-to-noise ratio, the instrument measures earthshine radiance spectra simultaneously in 60 effective fields of view (FOV), approximately transverse to the flight track, every 2 seconds (the CCD is read out every 0.4 s, and co-added in groups of 5), over a range of angles 57° either side of nadir. This gives a sufficient "push-broom" width to view the entire sunlit surface of the Earth, even in the tropics, with multiple orbital overlaps for much of the mid- to high-latitude regions.

During normal operations, OMI measures the solar irradiance spectrum once every 24 hours. The ratio of the earthshine radiance to solar irradiance, the *spectral albedo*, is calculated for each FOV. The OMI NO_2 retrieval algorithm is described in Section 3.

1.4. Data availability

The OMI NO_2 data product is available in a number of different geospatial forms:

- Level-2 orbital swath (L2);
- Daily global gridded, 0.25° × 0.25° (L2G);
- Station and regional overpass (OVP).

The L2 and L2G datasets and associated documentation are freely available through the NASA Goddard Earth Sciences Data and Information Services Center (GES-DISC, URL: `http://daac.gsfc.nasa.gov/Aura/OMI/index.shtml`).

The OVP data, generated daily for over 100 locations around the world, and also in support of validation and regional pollution studies, are available through the Aura Validation Data Center (AVDC, URL: `http://avdc.gsfc.nasa.gov/Data/Aura/OMI/OMNO2/`

---

[5] Department of Atmospheric Physics,

`index.html`). The subsetted data used for this paper were generated at the AVDC using the recommended usage quality flags [*Celarier et al.*, 2006].

Both the L2G and OVP data products are derived from the L2 data set, and not all of the fields found in the L2 data may be found in the derived data products. Complete details concerning the contents of the Level-2 files are available in *Veefkind and Celarier* [2006].

Each L2G file contains a $0.25° \times 0.25°$ grid data structure. Each cell of the grid contains a stack of data values for all the FOVs whose centers fell within that cell. For each FOV a subset of the available L2 fields is stored. Because it is organized geographically, the L2G data set should be suitable for users who wish to study specific geographic locations, as, for example, in the case of validation against ground based measurements, or for regional air quality studies.

Though all the data have been publicly released and are freely available, prospective data users are strongly encouraged to contact the principal investigators responsible for the data sets.

2. OMI Measurement

Atmospheric NO_2 column densities are retrieved using spectral measurements of the solar irradiance and earth shine radiance in the wavelength region 415–465 nm, using the instrument's VIS detector. The measurements are made with a spectral resolution of ~ 0.5 nm. Daily measurements of the solar irradiance have been made since the instrument became operational, with the exception of the period 2006 February 28 through 2006

Research Institute of Physics, St.

March 3, when a problem with the instrument's folding mirror prevented making daily irradiance measurements. Using measured irradiance spectra has resulted in the appearance of stripe structure in virtually all the data products, in which the retrieved quantities have different means at each of the 60 cross-track positions. This has necessitated the implementation of "destriping" algorithms.

The OMI instrument design and performance have been described by *Levelt et al.* [2006b, a]. *Dobber et al.* [2006] have discussed the calibration of the instrument, and the origin of the striping, or cross-track bias.

3. OMI Algorithm

In this section we present the essential details of the algorithm. A much more detailed description of the OMI NO_2 algorithm, its theoretical underpinnings, and uncertainty analysis may be found in [*Bucsela et al.*, 2006; *Boersma et al.*, 2002; *Wenig et al.*, 2007; *Boersma et al.*, 2004].

3.1. Slant column densities

The first part of the calculation of NO_2 columns consists in calculating the slant column densities. Since the OMI-measured radiance and irradiance spectra, and the laboratory spectra are all measured on different wavelength scales, the measured spectra are interpolated onto a common scale. The spectral albedo, R, is then fitted by a nonlinear least-squares technique onto the function

$$R(\lambda) \;=\; P_3(\lambda) \cdot \exp\left(-c_{\mathrm{NO2}} \cdot \sigma_{\mathrm{NO2}}(\lambda) - c_{\mathrm{O3}} \cdot \sigma_{\mathrm{O3}}(\lambda)\right) \cdot$$

Petersburg State University, St. Petersburg,

$$(1 + c_{\mathrm{ring}} \cdot \sigma_{\mathrm{ring}}(\lambda)) \ , \qquad (1)$$

where σ is the absorption cross section of the indicated species, and P_3 is a third-order polynomial in the wavelength, which models the component of the spectrum that is smoothly varying, due to Rayleigh and Mie scattering. Literature spectra are used for σ_{NO2} [*Vandaele et al.*, 1998], σ_{O3} [*Burrows et al.*, 1999a], and σ_{ring} [*Chance and Spurr*, 1997]. These spectra were convolved with a model OMI instrument slit function prior to use in the fitting algorithm. In all, each measured spectrum is subjected to a nonlinear least-squares fit with a total of seven free parameters (c_{NO2}, c_{O3}, c_{ring}, and the four coefficients in $P_3(\lambda)$). The algorithm also estimates the uncertainties in each of the fit parameters, as well as the χ^2 error and R.M.S. error of the fit.

The determination of the SCD does not include fitting to the absorption spectra of either H_2O or $O_2 - O_2$. The introduction of these species were found not to have a large effect on the retrieved NO_2 SCD, and resulted in longer execution times.

3.2. Initial vertical column densities

Initial estimates of the vertical column density (V_{init}) are calculated using AMFs derived from typical climatological profile shapes, with a nominal amount of NO_2 assumed in the troposphere ($\mathrm{AMF}_{\mathrm{init}}$). That is, the initial vertical columns are computed under the assumption that the troposphere is not polluted. The profiles assumed are a 1-year

---

Russia

average of daily profiles computed using the GEOS-CHEM model in the troposphere, and the Goddard Chemical Transport Model in the stratosphere [*Bucsela et al.*, 2006].

3.3. Stratosphere-troposphere separation

At the core of the OMI NO_2 algorithm is a procedure to identify fields-of-view (FOV) where there is significant tropospheric NO_2. This is required because the air mass factor depends upon the profile shape (though not the total amount, since the trace gas is optically thin): FOVs where there is significant tropospheric NO_2 require a different AMF to compute the VCD from the SCD. It is observed [*Gordley et al.*, 1996] that the stratospheric NO_2 field has relatively small gradients, particularly in the zonal direction. Our procedure for the stratosphere-troposphere separation essentially identifies the slowly-varying component of the total NO_2 field as the stratospheric field, and the rest as the tropospheric field.

Each orbit is treated as follows. The "target" orbit's data are read in, along with the data from all other available orbits that were measured within ±12 hours of the target. Each FOV is identified with a grid cell on a $1^\circ \times 1^\circ$ grid in latitude and longitude. For all the FOVs that are identified with a particular grid cell, a "cost" is computed from the initial AMF and uncertainty estimate for the V_{init}; the value of V_{init} having the lowest cost is saved in its associated grid cell. A "mask" identifying grid cells where there are known, persistent sources of NO_2 was developed for use in the algorithm; no V_{init} values are stored in masked grid cells. The V_{init} values are averaged in the meridional direction with a boxcar function of half width 5°. For each 1° latitude band, a wave analysis is

---

[6] CNRS, Route des Gatines, 91370

performed, fitting waves 0, 1, and 2, to give a preliminary background field. Grid cells whose V_{init} value exceeds the preliminary background field by more than one standard deviation are then excluded, and the wave analysis is redone. The result of this is a background field (V_{bg}) that has been influenced very little by the presence of regions of high NO_2 concentration. Since the V_{init} values were obtained using an AMF that is appropriate to a profile having most of the NO_2 in the stratosphere, no further correction to the background field is required.

3.4. Vertical column densities

For each FOV, the value of V_{init} is compared to the evaluated background field at that location. If V_{init} is less than the background field, then the final value of V (the total NO_2 column amount) is taken to be V_{init}. If V_{init} is larger than the background field, then the "polluted" part ($V_{\mathrm{init}} - V_{\mathrm{bg}}$) is scaled by the ratio $\mathrm{AMF}_{\mathrm{init}}/\mathrm{AMF}_{\mathrm{pol}}$, where $\mathrm{AMF}_{\mathrm{pol}}$ is obtained using the climatological GEOS-CHEM-modeled profile [*Bey et al.*, 2001; *Martin et al.*, 2002]. This procedure gives the total column, the background column, and the polluted column. In addition, a tropospheric column, equal, in the polluted case, to the polluted column plus the amount of the unpolluted profile that exists below the tropopause (assumed to be at 200 hPa). Finally, if, according to the standard cloud product, the cloud fraction is

---

Verrières le Buisson, France

larger than 0.1, then the “below cloud amount” (the amount of NO_2 that is inferred to be below the visible surface of the clouds) is also computed.

3.5. Destriping

Due to radiometric calibration and dark-current drift in OMI’s CCD detectors, which affects the radiance measurements differently from the irradiance measurements, nearly all OMI Level-2 data products show some degree of cross-track bias, which appears as stripes of systematically elevated or diminished values at certain cross-track scan positions, persisting throughout each orbital track [*Dobber et al.*, 2006]. While the origin of much of the cross-track bias is now understood, and an improvement in the Level-0 to Level-1 processing algorithm is being implemented, the data available for the purpose of validation to date have had significant cross-track bias.

A “destriping” procedure has been implemented in the OMI NO_2 algorithm. In this procedure, the NO_2 SCDs and AMFs are collected for the 15 orbits (or fewer, depending on data availability) used to construct the background field. These are then used to construct separate SCD correction offsets for the northern and southern hemispheres:

$$\Delta_i = \overline{\mathrm{SCD}_i} - \overline{\mathrm{AMF}}_i \cdot \frac{\langle \mathrm{SCD} \rangle}{\langle \mathrm{AMF} \rangle} \,, \tag{2}$$

where i is the cross-track scan position (1 to 60), the overlines indicate averages for single scan positions, and angle-brackets indicate averages over all scan positions. The Δ_i are subtracted from the SCDs before applying the final air mass factors.

One concern about this procedure has been that it could introduce an unknowable bias in the computed NO_2 column densities. This will be discussed in light of the ground-based

---

[7] Chemistry and Physics of Atmospheres,

validation data. Another concern is that it is observed that, even using this procedure, there is some residual striping in the data. The data that have severe bias are generally flagged (and so not used in the validation). We assume that the residual biases are small, and are sufficiently symmetrically distributed, that the biases cancel: The cross-track biases change from orbit to orbit, and successive overpasses of any site are viewed with different FOVs.

4. Validation of OMI NO_2 columns

4.1. Stratospheric column

4.1.1. SAOZ and DOAS instruments in the NDACC network

The NDACC (Network for the Detection of Atmospheric Composition Change) is an international cooperative network that coordinates the operations and data analysis at more than 30 stations at various latitudes on the globe from 76°S to 79°N. The ground-based UV-Visible zenith-sky spectrometers include both SAOZ (*Système d'Analyse par Observations Zénithales*) as well as DOAS instruments, which provide ozone and NO_2 vertical columns at sunrise and sunset using the Differential Optical Absorption Spectroscopy (DOAS) technique [*Platt*, 1994] in the spectral range 410–530 nm. Zenith-sky measurements made at solar zenith angles between 86–91° are averaged to give estimates of the column NO_2. Because of the optical geometry of the measurement, the retrieved NO_2 column is much more sensitive to the stratospheric NO_2 column than to the tropospheric column. Most of the instruments are located in remote geographical regions, far from any significant source of tropospheric NO_2. Figure 1 shows the geographical distribution

---

Federal Space Pole, Belgian Institute for of the SAOZ stations that are operated by the French *Centre National de la Recherche Scientifique* (CNRS). Only the instruments at the Observatoire Haute-Provence (OHP), France, and Bauru, Brazil, are in any proximity to presumed anthropogenic sources of NO_2. Measurements from the SAOZ instruments have been previously used to compare with NO_2 measurements by the space borne GOME [*Burrows et al.*, 1999b] and SCIAMACHY [*Bovensmann et al.*, 1999] instruments [*Ionov et al.*, 2006a, b, 2007; *Piters et al.*, 2006; *Lambert et al.*, 2001].

Stratospheric NO_2 exhibits a pronounced diurnal cycle due to its daytime photolysis into NO and nighttime conversion into N_2O_5. The NO_2 daily cycle starts with a fast drop shortly after sunrise, followed by a quasi-linear slow increase during the day, a fast increase at sunset, and finally a slow decrease during the night. The time-dependence of the stratospheric NO_2 concentration has important implications for the validation of the space based NO_2 measurements. If the ground based measurements are not collocated in time with the OMI measurements, they need to be corrected, using photochemical and transport models, to account for the time difference. In addition, if the ground-based measurements entail an optical path that is more horizontal than vertical, view and solar geometries must be taken into consideration when identifying “collocated” measurements.

The diurnal cycle has been simulated with a photochemical box model derived from the SLIMCAT 3D chemical-transport model [*Denis*, 2005]. It includes 98 chemical and 39 photochemical reactions, including heterogeneous chemistry on liquid and solid particles. Calculations are made at 17 altitude levels with a time step of 1 minute. The NO_2 total column is obtained by integrating the profile assuming a constant density in each layer.

Space Aeronomy, 3 Avenue Circulaire,

Figure 2 shows the results of simulations at two SAOZ stations, OHP at mid-latitude and and Scoresby Sund in the Arctic, for spring and fall. Using this photochemical model, a

---

B-1180 Brussels, Belgium

[8] Laboratory for Atmospheric Research,
Dept. of Civil and Environmental
Engineering, Washington State University,
Pullman, WA 99164-2910, USA

[9] Science Division, NASA Jet Propulsion
Laboratory, California Institute of
Technology, Pasadena, CA 91109

[10] Netherlands National Institute for
Public Health and the Environment
(RIVM), Bilthoven, The Netherlands

[11] Institute for Environmental Physics,
University of Bremen, D-28334 Bremen,
Germany

[12] Max-Planck-Institute for Chemistry,
Mainz, Germany

[13] Institute for Environmental Physics,
University of Heidelberg, D-69120
Heidelberg, Germany

diurnal time series of the ratio $NO_2(\text{sunrise})/NO_2(t)$ was calculated for each month, and at each SAOZ location. As SAOZ is an average of measurements between 86° and 91° SZA the NO_2 column at 88.5° SZA is taken as the sunrise reference. The OMI stratospheric measurements (total minus tropospheric columns) were calculated and then normalized to corresponding sunrise values using these ratios.

The optical geometry of the twilight SAOZ measurements is such that the light paths traverse rather large distances through the stratosphere, so the stratosphere is sampled at some distance from the measurement site. This should be taken into account when seeking "match up" satellite FOVs corresponding to the ground-based measurements, especially in regions with large stratospheric NO_2 gradients. However, in the present studies, a simpler approach was adopted, in which the match up criterion was that the ground site was within an OMI field-of-view. If multiple match ups are identified for a single day, the one whose center fell closest to the ground station was used.

Finally, the OMI NO_2 algorithm provides total column NO_2, and the tropospheric column NO_2. Since SAOZ measurements are roughly 50 times as sensitive to the stratospheric column as to the tropospheric column, it is of interest to compare the SAOZ-derived values to the difference of the total and the tropospheric columns.

Figure 3 shows the time series of the difference between the sunrise SAOZ measurements and the matching OMI measurements from eight SAOZ sites, adjusted to account for the difference between the satellite overpass time and sunrise. The statistical characteristics of these differences are presented in Table 1. Besides a comparison to just the stratospheric column, the table presents a comparison between the OMI total column and the SAOZ instrument measurements. It is seen that, at virtually all latitudes, there is very good agreement, on average, between the ground-based and satellite-based measurements of the total stratospheric NO_2 column. However, a small annual cycle is apparent in the time-series for the higher latitudes, with lower values in the winter than in the summer. This cycle, which appears in both the northern and southern hemisphere high latitudes, may be related to the OMI sampling under those conditions, or may reflect a sensitivity to the choice of matching OMI FOV corresponding to a given ground-based observation, or may be due to a bias either in the satellite measurement at high solar zenith angle, or in the ground-based measurements as the sunrise azimuth tends poleward. While the influence of the seasonal cycle on the overall statistics is fairly small, understanding it may be an avenue of further study.

The correlation coefficients between the SAOZ and OMI-measured stratospheric NO_2 columns are better, and the mean absolute differences smaller, for the mid-to-high latitude sites than for the tropical sites. Since the stratospheric NO_2 concentrations are smaller in the tropics in the first place (annual mean of about $2.5 \times 10^{15}\,\mathrm{cm}^{-2}$, compared to an annual mean of $4 - 5 \times 10^{15}\,\mathrm{cm}^{-2}$ at the high latitude sites), the *relative* differences are much greater in the tropics, and even the mid-latitude sites (OHP and Kerguelen), than at the high-latitude sites.

4.2. Tropospheric column

4.2.1. MAX-DOAS

The MultiAxis DOAS (MAX-DOAS) technique is an extension of the zenith-sky DOAS technique described in Section 4.1.1, but having much greater sensitivity to lower tropospheric layers. In brief, a MAX-DOAS typically consists of two main parts: A grating spectrometer mounted inside a thermostatted box that is located inside a building, and one or more scanning telescopes connected to the spectrometer via fiber optics. Consecutive measurements at increasing elevation angles are performed in an acquisition cycle that always contains observations at a number of low elevations, and a zenith observation.

From each of the measurements, a slant column is retrieved using the DOAS method described in Section 4.1.1[*Platt*, 1994]. Besides NO_2, a number of other absorbers, plus the Ring effect, are included in the fit, as are a multiplicative polynomial and an additive polynomial for stray light correction. In order to account for the temperature dependence of the NO_2 absorption spectrum, a second cross-section (295 K and 221 K) may be introduced in the retrieval to improve the fit and correct the derived vertical column. Some groups use one-temperature retrievals, while other groups use two-temperatures, and this may cause some discrepancy between the MAX-DOAS instrument results. In contrast, the OMI retrieval uses a single temperature, and applies a height-dependent temperature correction, based on climatological temperature profiles, in the calculation of the AMFs[*Bucsela et al.*, 2006; *Boersma et al.*, 2002].

The lowest-elevation measurements have a large sensitivity to absorption in the boundary layer, while the zenith measurements are used as background reference spectra which contain Fraunhofer structures and the stratospheric absorption features. Since photon scattering largely occurs below the tropopause, the photons collected from different elevation angles have essentially the same stratospheric path, but different light paths in the troposphere. The difference between successive off-axis line-of-sight (LOS) and zenith measurements is therefore only sensitive to the troposphere. For NO_2 retrieval, radiative transfer simulations show that under polluted conditions, the stratospheric contamination is generally smaller than 1%. A more in-depth description of the MAX-DOAS measurements, as they were done at the DANDELIONS campaign, can be found in *Brinksma et al.* [2007].

During the DANDELIONS campaigns [*Brinksma et al.*, 2007], various MAX-DOAS instruments operated quasi continuously from the Cabauw Experimental Site for Atmospheric Research [*Russchenberg et al.*, 2005] throughout May through mid July 2005 and throughout September 2006. These instruments were provided and operated by BIRA-IASB, the University of Bremen, and the University of Heidelberg.

The Heidelberg MAX-DOAS instrument differs from the others in that it has a set of three movable telescopes, which enable simultaneous measurement cycles in three azimuth viewing directions *Wagner et al.* [2004]).

For the Bremen instrument [*Wittrock et al.*, 2004], the zenith direction is viewed without a mirror, while the other elevation angles in the measurement cycle are selected through a rotating mirror inside the telescope. The range of elevation angles is $0° - 30°$. In the 2006 DANDELIONS campaign, separate UV and VIS instruments were operated by the Bremen group.

4.2.2. Agreement Between MAX-DOAS Instruments

The level of agreement achieved between the MAX-DOAS instruments is quantitatively summarized in correlation plots (Fig. 4) where tropospheric NO_2 columns from the BIRA instrument are compared to those from the other groups, for the 2005 campaign. This comparison is useful because there are differences between the instruments and their data reduction procedures, and because instruments viewing different directions can be used to detect directional dependences of the measurements. Very good agreement is found between the BIRA and Bremen data sets (correlation coefficients of 0.9 and slope of 1.1), and also between BIRA and the three Heidelberg telescopes (correlations between 0.82 and 0.91), especially considering that the BIRA instrument was 200 m away from the other two instruments.

When the BIRA and Heidelberg data sets were re-retrieved using identical NO_2 absorption cross-sections, an even better agreement is found, reaching a correlation coefficient of 0.92 and a slope of 0.99. This level of agreement is only achieved when considering the southwest-pointing Heidelberg telescope: this is approximately in the same direction as the two other instruments. This highlights the degree to which horizontal inhomogeneities in the NO_2 field can strongly affect the agreement between ground based and satellite based measurements.

4.2.3. Heterogeneity of the NO_2 Field

If the tropospheric NO_2 layer were horizontally homogenous, the observed NO_2 SCDs for the different azimuth angles observed from the three telescopes of the Heidelberg instrument would have been similar. The horizontal inhomogeneity of the NO_2 concentration field can be estimated from the observed differences among the various viewing directions. Estimating the horizontal inhomogeneity is very important for the validation of satellite instruments with ground based observations. In the presence of strong horizontal gradients, ground based observations may not be representative for the average value within a satellite ground pixel.

Since the horizontal extent of the absorption paths along the line of sight is largest for low telescope elevation, those at 3° were used to estimate the heterogeneity of the tropospheric NO_2 concentration field. This was done by evaluating the SCD in the three azimuthal viewing directions at 3° elevation, and calculating the ratio of the maximum and the minimum. A horizontally homogenous concentration field yields a ratio of one; the more this ratio deviates from unity, the larger are the horizontal gradients. In addition to the strength of the horizontal gradients, the direction of the NO_2 gradient was estimated, though in a limited way, since the Heidelberg MAX-DOAS was measuring in only three azimuth directions. Fig. 5 displays the time series of the ratios at daily noon. High ratios indicate strong gradients, and the color of the points indicates the direction of positive gradient.

To interpret the retrieved information on the gradient of the tropospheric NO_2 concentration field, it is important to consider two effects that can affect the observed SCDs, especially for low elevation angles: First, the sensitivity to the relative azimuth angle (between the telescope and the sun). This dependency becomes more pronounced for increasing solar zenith angle (SZA) and increasing aerosol load [*Wagner et al.*, 2004]. Second, the effect of the atmospheric aerosol load on the atmospheric visibility, and thus on the horizontal extents of the absorption paths along the line of sight. Thus, depending on the aerosol load, the calculated ratio represents information on gradients over areas of different horizontal extent. The dependence on the azimuth angle was found to be below 15%, for SZA between 20° and 80°. Almost all observed ratios of the maximum and minimum NO_2 SCDs (see Fig. 5) were much larger than this. Effective path lengths are enhanced by aerosols above about 1 km, and diminished by aerosols below 1 km. For an elevation angle of 3°, the effective path length is about 19 km in a pure Rayleigh-scattering atmosphere, but this can be reduced to as little as 4.5 km by surface-level aerosols, or enhanced to 25 km by higher-altitude aerosols [*Brinksma et al.*, 2007; *Deutschmann and Wagner*, 2006; *Wagner et al.*, 2007, 2004].

4.2.4. Comparisons with OMI tropospheric NO_2

The different MAX-DOAS data sets are compared to the OMI Level-2 cloud-free data (O_2–O_2 cloud fractions in the OMI products less than 20%) for 2005, in order to produce the correlation plot presented in Figure 6 and Table 2. The MAX-DOAS data were linearly interpolated to the satellite overpass time.

The OMI tropospheric vertical columns were generally distributed from 0 to about 2.5×10^{16} cm^{-2}. In one case the ground based MAX-DOAS column (3×10^{16} cm^{-2}) significantly exceeded the corresponding satellite values, possibly due to a local enhancement of the NO_2 concentration at Cabauw. Because of its obvious anomaly, this point has been excluded from the regression analysis.

The regression analyses show that similar results were achieved with the BIRA and the Bremen data sets, the correlation coefficient between ground based and satellite data being about 0.6. A lower correlation was obtained with the Heidelberg data when considering only the southwest direction measurements (closest to the viewing direction of both Bremen and BIRA instruments), possibly due to the smaller number of coincidences with this instrument, and also the shorter integration time used, which may increase the sensitivity to local inhomogeneities in the NO_2 field. In order to further explore the impact of possible horizontal smoothing effects on the comparison results, the Heidelberg measurements simultaneously recorded from all three directions have been averaged and again compared with satellite data. The resulting correlation coefficients, also given in Table 2, have significantly improved and are now the highest of the three MAX-DOAS instruments. This suggests that the scatter in MAX-DOAS versus satellite comparisons is, indeed, largely dominated by the difference in their spatial and temporal averaging.

As is evident from the regression results, the OMI tropospheric NO_2 columns seem to be systematically lower than the MAX-DOAS results, for both OMI products considered. However, it must be noted that the correlation coefficients are rather poor in all cases, which might be due to several reasons including uncertainties in both ground based (geometrical approximation) and satellite retrievals (AMF sensitivity to errors in aerosols, clouds and NO_2 profile shape). However, the slopes are poorly determined, due to the small number of poiints and the large data scatter.

4.3. Total column

4.3.1. Brewer

Cede et al. [2006] have described a method for retrieval of total-column NO_2 from direct-sun measurements using a Brewer MK-III double monochromator spectrophotometer. The Brewer MK-III instrument was primarily designed to make measurements of ozone from wavelengths below 320 nm, and can measure spectral irradiance and radiance from 285 to 365 nm. Its measurement modes include a spectral scan mode, where the gratings are moved and any wavelength can be selected, and a slit mask mode, in which a slit mask is introduced in the optical path allowing nearly simultaneous measurements at 6 wavelengths, spaced about 3 nm apart. The spacing of the slits in the slit mask was chosen to optimize the ozone retrievals between 303 and 320 nm, but in the 345–365 nm range the measured wavelengths fall very nearly on maxima and minima in the NO_2 absorption spectrum (see Figure 7), which permits the retrieval of total column NO_2. These measurements have been made at the NASA Goddard Space Flight Center, on a nearly continual basis since August 2004, with measurements made every half hour during the sunlit hours.

The retrieved NO_2 columns have a large instrumental noise, so data must be averaged over several hours time in order to make meaningful comparisons to the OMI-measured values. However, the location of the instrument, 3 km from the Washington Capital Beltway and 2 km from the Baltimore-Washington Parkway, on the outskirts of a major metropolitan area, is such that there are often substantial sub-hour time variations in the actual tropospheric NO_2 concentrations. The combination of the intrinsic variability of the measurements with the frequent occurrence of significant actual concentration variations within a given time-window used for collocation with OMI overpasses complicates the process of using the Brewer data for validation of OMI NO_2 measurements. Comparisons having useful statistical significance can be made using monthly averages of the Brewer and OMI datasets.

Figure 8 shows the comparison between the monthly mean Brewer-measured and OMI-measured NO_2 columns. In the Washington DC area, early afternoon NO_2 columns are dominated by the boundary layer columns. The difference that is seen, with OMI-measured columns that are about 35% smaller than the Brewer-measured columns, can thus be largely attributed to the tropospheric NO_2. In Figure 9 the daily and monthly mean values are plotted, along with the line of linear regression to the monthly means. The regression analysis, performed on the monthly means, and weighted according to the standard deviations, gives a slope of 0.67, with a correlation coefficient $R = 0.95$.

4.3.2. MultiFunction DOAS (MFDOAS) measurements

The MF-DOAS instrument observes scattered skylight with a 1° vertical FOV at varying viewing azimuth and elevation angles, as well as direct sunlight in the UV-visible spectral region. From these measurements are retrieved NO_2, O_3, SO_2, and CH_2O slant columns. The MF-DOAS spectrograph is a single pass commercial Czerny-Turner spectrograph of focal length 300 mm. The instrument covers a wavelength range from 280 nm to 490 nm with a spectral resolution of 0.82 nm (6 pixels FWHM). Scattered sky light is collected by a 12 cm telescope and passes into the spectrograph through two filter wheels that contain depolarizers, spectral flattening filters, and UV cutoff filters. Direct sunlight is fed into a spectralon integrating sphere of diameter 8 cm before passing through the filter wheels and results in a signal level similar to that from the scattered sky. A two-dimensional CCD detector (512 × 2048 pixels) is used in the focal plane. Spectrograph stray light is reduced by a spectral flattening filter, which reduces the long wavelength throughput of the instrument relative to the short wavelength signal. A solar tracker moves the entire instrument for positioning and sun tracking. An instrument schematic is presented in Figure 10.

This ground-based MF-DOAS instrument was fielded in a prototype form during the INTEX-B campaign for Aura/OMI validation. It was positioned on the roof of a building at Pacific Northwest National Laboratory in Richland, WA (PNNL; 46.3409°N, 119.2787°W), located in an urban area known as Tri-Cities (the merged cities of Kennewick, Pasco and Richland, WA) with total population of approximately 150,000 in an area of 250 km^2. PNNL is situated approximately 15 km north of the center of Richland, and northwest of the area's population center. The major source of local NO_2 pollution is vehicular exhaust.

NO_2 differential slant columns (DSCD) were derived using the DOAS technique, based on Beers law. A nonlinear least squares algorithm was used to fit our measured spectral cross sections of NO_2, O_3, instrument spectral polarization, and Ring effect in the spectral region 400–419 nm. A polynomial was included to remove slowly varying Rayleigh and Mie scattering spectral shapes. The reference solar spectrum used for the data analysis was measured at zenith at local noon on April 30, 2006, a day with very low pollution levels. Raw spectra were corrected for detector dark background and flat field. Figure 11 shows typical residual optical densities after the least squares fitting procedure for observations taken on May 9, 2006 at 5° elevation and 4 azimuth angles. The LIDORT radiative transfer code [*Spurr*, 2001; *Spurr et al.*, 2001] was used to calculate the air mass factors (AMF) to convert the DSCD to vertical column density (VCD). As an example of the results, Figure 12 presents the spatial and temporal variation of NO_2 differential slant column for May 9, a polluted day. Higher column densities were observed to the south and east, toward the urban center, as expected. Measurements taken at 5° elevation showed higher NO_2 tropospheric column compared to 15° and 45° angles, as expected. These elevated NO_2 slant column densities were particularly pronounced during the morning rush hour.

The Aura satellite flies over Tri-Cities area around 1330h with spatial resolution approximately 13 km × 24 km. Figure 13 shows contour plots of OMI tropospheric NO_2 VCD for May 9, derived from the Level-2 OMI data product. OMI tropospheric NO_2 vertical column densities "integrated" over several pixels in the MF-DOAS observation direction were compared to MF-DOAS tropospheric NO_2 VCD using *a priori* differential AMFs for clear days at PNNL from the LIDORT radiative transfer code. Figure 14 shows results for the time period April 30 through May 13, 2006, with reasonable correlation observed for these clear days.

The slope of the data in Figure 14 shows that OMI determinations of tropospheric NO_2 VCD are 0.81 ± 0.11 of that determined from MF-DOAS with a correlation coefficient R^2 of 0.92. Thus, OMI measures a somewhat smaller VCD than that determined from MF-DOAS.

4.3.3. Pandora-1 Direct Sun DOAS measurements

The lightweight, portable Pandora-1 spectrometer system measures direct-sun irradiances from 270 to 500 nm at ~ 0.5 nm resolution. The outdoor head sensor is mounted on a tracking system and holds a single strand fiber optic cable, which collects the light passed through a collimator (1.6° FWHM field of view) and a filter wheel. The other end of the fiber is connected to a 75 mm focal length symmetric Czerny-Turner grating spectrometer using a 1024×1 pixel CMOS detector, stabilized to $20° \pm 1$. The total NO_2 column is retrieved by the DOAS method, in the 400–440 nm window, using a fixed reference spectrum determined from Pandora-1 data obtained over an extended period of at least 2 weeks. To estimate the NO_2 amount in the reference spectrum, a bootstrap method as described in *Cede et al.* [2006] was applied, on the assumption that a few measurements were obtained when there were low tropospheric NO_2 amounts (e.g., just after sunrise). Figure 15 shows Pandora-1 data during the SCOUT campaign in July 2006 at Thessaloniki, Greece. Excellent agreement is seen between the OMI and Pandora-1 measurements, though the OMI overpass times seem to occur just before or just after the mid-day maximum in NO_2 concentration; this limits the range of NO_2 concentration values explored in this comparison. A number of further field campaigns are planned, during which Pandora-1/OMI comparisons will be done.

4.3.4. Direct Sun DOAS (BIRA)

During the second DANDELIONS campaign, a direct-sun DOAS instrument was operated in addition to the MAX-DOAS instrument. The well-defined optical path and air mass factor make this instrument equally sensitive to absorption along the whole optical path and so provides accurate NO_2 total columns.

The instrument is similar in concept to the MAX-DOAS: Inside the building, in a thermo regulated box, a grating spectrometer covering the UV-Vis region is coupled to a cooled CCD detector, connected by depolarizing fiber optic bundle to the external optical head. Outside, alongside the MAX-DOAS scanning telescope, a collimating optic tube is mounted on a BRUSAG commercial sun-tracking system, holding the fiber.

The retrieval is also done using the DOAS approach: The ratios of the measured radiance spectra to a reference spectrum are analyzed with respect to a set of reference spectra, in the 425–450 nm window, including laboratory spectra of O_3, H_2O, O_2-O_2, the computed the Ring effect spectrum, and NO_2 cross-sections at two different temperatures. In contrast to the analysis of MAX-DOAS data, a fixed reference spectrum (measured on 7 September 2006) has been used for the whole time-series. The NO_2 residual slant column amount included in this reference spectrum has been obtained by analysing it with respect to the Kurucz solar atlas [*Kurucz et al.*, 1984], which was assumed to be free of NO_2 absorption. The Kurucz solar spectrum was convolved with a precisely measured instrument slit function to match the instrument's spectral resolution. Based on this analysis, total absolute slant columns could be derived from direct sun measurements; these were transformed into total vertical columns using geometrical AMFs.

Figure 16 shows the time series for the BIRA DOAS measurements of the total column NO_2 (filled dots), which provides a good idea of the diurnal variation of NO_2 levels. The open squares show the collocated OMI measurements (one or two per day). The OMI snapshots of vertical column NO_2, for the most part, appear to be in quite good agreement with the ground-based measurements. Note that the OMI data are filtered for clouds (cloud fraction $\leq 20\%$).

Figure 17 shows the correlation plot of the collocated data (the point nearest in time to the OMI overpass). A linear regression, constrained to pass through the origin, gives a slope of 0.84 ± 0.05. The scatter in the data ($R = 0.68$), and the relatively small number of data points ($N = 26$)do not permit a statistically significant estimation of an additive bias.

4.3.5. FTUVS measurements at Table Mountain, California

Another instrument that has been used to validate OMI NO_2 total column measurements uses the Fourier Transform Ultraviolet Visible Spectrometer (FTUVS), a UV-VIS-NIR interferometer, at the Table Mountain Facility (TMF), north of Los Angeles, California, at 34°22.9′ N, 117°40.8′ W, at an altitude of 2290 m (7300′) [*Cageao et al.*, 2001]. Spectra are recorded in the direct solar absorption mode with a spectral resolution of 0.0013 nm, which is sufficient to resolve NO_2 vibronic features. By measuring the doppler-shifted spectra from the east and west solar limbs, and taking the ratio of the two, one can remove the solar Fraunhofer lines; there is no need to measure a high-sun reference spectrum, as in a number of the other methods described in this overview.

The instrument is not readily transportable. The FTUVS observation site overlooks the Antelope Valley, north of the Los Angeles Basin. This area is characterized by relatively clean air under most conditions, but is often influenced by polluted air from Los Angeles in the afternoon, advected through the Cajon Pass. While considerably above the tropospheric background under these conditions, the NO_2 column abundance values rarely exceed 1×10^{16}molecules cm^{-2}, which is considerably smaller than values measured directly downwind of a polluted urban area (see Fig. 8). Because the altitude of TMF is about 2500 feet above the Antelope Valley, FTUVS column abundance measurements of NO_2 will be biased relative to the center of the OMI footprint. The bias is small relative to the total column, and will not have a significant effect on the slope of the OMI-FTUVS correlation. The OMI data used for validation were sorted by distance from the TMF site, in order to mitigate somewhat the possible effects of the distribution of elevations within a FOV. It was found that a minimum distance of about 10 km is required for good intercomparison.

The FTUVS instrument time is shared with other Aura validation activities. On average, measurements were acquired twice a week over the period March–November, 2006.

The slant column NO_2 amounts are retrieved by fitting the measured absorption spectra to laboratory spectra at a number of temperatures [*Nizkorodov et al.*, 2004], in windows containing 10 to 20 NO_2 rotational lines. Geometric AMFs were used to convert the SCDs to VCDs. Figure 18 presents the comparison of the OMI-derived and FTUVS-derived measurements of total column NO_2. In this figure, the points where the OMI FOV center fell within 10 km of the Table Mountain Facility site are colored red. The linear regression line shown is fit only to those points. As shown, this line has a slope of 0.77 ± 0.41, and it does not go through the origin. This data set suggests that the OMI NO_2 totals are underestimated in the middle of the data range, but that there may also be a positive additive bias.

4.4. NO_2 Profile measurements

As pointed out in previous sections, and in *Boersma et al.* [2002] and *Bucsela et al.* [2006], the shape of the vertical profile of NO_2 influences the (physical) air mass factors. The OMI NO_2 algorithm uses a set of assumed profiles, which were derived from model studies; these assumed profiles thus affect the retrieved total and tropospheric NO_2 amounts. It is therefore important to evaluate how well the assumed profiles approximate the actual profiles, *vis-à-vis* the air mass factor calculation. There have been very few efforts to measure NO_2 profiles [*Heland et al.*, 2002; *Martin et al.*, 2006]. Recent efforts include measurements during the September 2006 DANDELIONS campaign (lidar, *in situ* at two altitudes, and MAX-DOAS at two altitudes, see section 4.4.1), and aircraft-based *in situ* measurements taken during the INTEX-B campaign in North America.

4.4.1. NO_2 lidar

NO_2 profiles were measured by a lidar system, developed at RIVM, during the DANDELIONS campaign in September 2006 [*Brinksma et al.*, 2007]. The lidar consists of an emitter and a receiver unit. The entire system is housed in a truck, constituting a fully self-supporting mobile laboratory. The emitter unit consists of a pulsed pump laser-dye laser combination, running at 30 Hz. The dye laser is tuned to 449.10 nm and detuned to 448.31 nm every other pulse. The latter wavelength is absorbed more strongly by NO_2

than the former. The laser pulses, 40 mJ in energy, 10 ns in duration, are directed into the atmosphere, where they are scattered by gas molecules and aerosol particles. The receiver unit collects the backscattered light, through a 280 mm telescope, onto a photomultiplier tube, with an interference filter to block daylight. A digitizer samples the signals with a range resolution of 3.75 m.

The NO_2 concentration at a certain altitude is derived from the log of the ratio of the backscattered signals at the two wavelengths, using the differential absorption lidar (DIAL) method. Since the laser pulses are not emitted from the center of the telescope, the laser beam is not in view of the telescope at close range, and thus the lidar is effectively blind for the first 500 m. When measurements starting near the surface are required, the emitter section and receiving telescope are tilted through various elevation angles; the measurements are combined into a single profile, where elevations close to the horizontal yield NO_2 concentrations at low altitudes but pertaining to a certain horizontal extent away from the instrument (for a near-horizontal measurement, typically about 2500 m), while a zenith observation is performed exactly above the truck. Completing one vertical profile typically takes 50 minutes, providing data in a altitude range of a few meters up to approximately 2500 m, with an accuracy of $0.2 - 0.4\ \mu\mathrm{g\,m^{-3}}$. Range and accuracy depend on atmospheric conditions. The vertical resolution of a profile varies, and typically is about 15 m at the lowest altitude, increasing to over 500 m at the highest altitude. The resolution arises from averaging of data over an altitude range, based on signal-to-noise considerations.

A paper describing the lidar and other time-resolved three dimensional observations of NO_2 during the 2006 DANDELIONS campaign is in preparation (H. Volten et al., in preparation).

Figure 19 presents examples of profile measurements for a relatively clean day, September 9, 2006, and for a polluted day, September 12, 2006; in both cases, there was little-to-no cloud cover. The concentration of NO_2 is high at ground level, and drops to zero (within the accuracy of the measurement) above the boundary layer. The boundary layer heights, provided by the boundary layer lidar at Cabauw, are indicated in Figure 19 by a dashed line. The figure shows that the day-to-day variations in NO_2 at the surface may be considerable, from around 3 μg NO_2 m^{-3} on a clean day to more than 50 μg NO_2 m^{-3} on a polluted day. Large diurnal variations may also occur.

4.4.2. In-situ aircraft measurements

In situ measurements of NO_2 from the DC-8 aircraft were obtained during the INTEX-A (summer 2004), PAVE (winter 2005) and INTEX-B (spring 2006) campaigns. These have been discussed by *Bucsela et al.* [2007]. The NO_2 profiles from these experiments are useful for validating both the shapes of the model profiles used in the OMI retrieval algorithm, and, in turn, the tropospheric column amounts from the satellite retrievals. The aircraft profiles obtained during INTEX-A and PAVE were combined into composite land and ocean profiles. The *in situ* profiles were seen to be very similar to the annual mean GEOS-CHEM profiles used to retrive tropospheric NO_2 columns from OMI, and the AMFs computed from the measured profiles were slightly larger than those calculated using the model profiles.

A more quantitative analysis was performed using a set of approximately 70 profiles measured during INTEX-B. Error-weighted linear regressions comparing the AMFs yielded a slope of 1.10 ± 0.10 (*in situ* profile AMF greater than that used by the OMI algorithm). This means that the OMI VCD would overestimate the actual VCD by 10%(±10%).

In situ measurements of NO_2 can also be used to validate tropospheric column amounts from OMI. The INTEX-B data were used for this analysis by *Bucsela et al.* [2007] (see also *Boersma et al.* [2007]). Two representative profile analyses are shown in Figure 20. The full set of profiles from INTEX-B where used The correlation between the aircraft and OMI data sets was good ($R = 0.83$). This comparison is shown in Figure 21. The integrated *in situ* tropospheric columns were found to be somewhat larger than the OMI Level-2 columns, as indicated by the slope of 1.10 ± 0.08. Although some of the *in situ* columns required significant extrapolations, sensitivity studies indicated that the overall results were generally robust with respect to the choices made for the profile binning, integration and extrapolation, as well as being relatively insensitive to the errors assumed for the weights. The insensitivity to extrapolation is consistent with findings in a similar aircraft study by *Heland et al.* [2002].

5. Conclusions and discussion

This paper has presented a number of results of experiments where ground- and aircraft-based measurements of NO_2 can be compared with collocated measurements and retrieval by OMI. Since some measurements estimate the stratospheric column, others the tropospheric column, and still others the total column, their results can be used to validate the OMI NO_2 standard data product's estimates of these columns.

Table 3 summarizes the results of the numerous validation studies that have been discussed in this overview.

On the basis of the SAOZ and DOAS measurements, which are most sensitive to the stratospheric NO_2 columns, the OMI stratospheric NO_2 appears to agree with the ground-based measurements to within $\sim 10\%$.

The OMI tropospheric column appears to be consistently lower than the various ground-based measurements, though there is some inconsistency amongst those ground-based measurements. Though many of the various instruments and methods for measuring tropospheric and total NO_2 have not themselves been validated, it is noteworthy that they all give NO_2 estimates that are on average greater than those retrieved from OMI. This may indicate a bias in the OMI retrieval. However, a number of cases have been studied, where average differences between OMI and ground based measurements decrease as the geographic match up criterion is tightened. It is likely to be due to the inhomogeneity of the tropospheric NO_2 field, and, in particular, the fact that ground-based measurements are often made in or near regions of moderate to strong sources of NO_2: The OMI FOV that includes the site will also include a substantial ($\sim 10^2$ km^2) regions where much lower NO_2 concentrations prevail. The was borne out in the Brewer studies [*Cede et al.*, 2006] and in the correlation studies of *Veefkind et al.* [2007] (see also Section 1.) However, the data taken at TMF (Section 4.3.5) were mostly obtained under conditions of relatively clean tropospheric air, and these data also suggested a negative bias for OMI retrieval.

Potential biases can arise at any of the steps in the algorithm. Instrumental artifacts are known to give rise to the cross-track bias (striping) and the destriping process can certainly give rise to a general bias. The stratosphere-troposphere separation is based on an initial AMF, and any bias in that AMF will result in a bias in the background (mostly stratospheric) field. After the stratosphere-troposphere separation, a new AMF is constructed, based on model-based-climatology derived *a priori* profiles. The aircraft *in situ* measurements of NO_2 profile shape suggest that the *a priori* profile shapes are essentially correct, in that the two do not give appreciably different AMFs. The AMF is also sensitive to the surface albedo. The OMI algorithm uses a climatological surface albedo, and this may be a worthy subject for future validation studies.

It should be mentioned that all the validation studies reviewed here focused on mostly cloud-free conditions. However, while OMI FOVs are considerably smaller than those of earlier atmospheric remote sensing instruments, they are still large enough that very few can be expected to be completely uncontaminated by clouds.

Acknowledgments

Part of this research was carried out at the Jet Propulsion Laboratory, California Institute of Technology, under contract with the National Aeronautics and Space Administration.

References

References

Bey, I., D. J. Jacob, R. M. Yantosca, J. A. Logan, B. D. Field, A. M. Fiore, Q. Li, H. Y. Liu, L. J. Mickley, and M. G. Schultz (2001), Global modeling of tropospheric chemistry with assimilated meteorology: Model description and evaluation, *J. Geophys. Res.*, *106*, 23 073–23 096.

Boersma, K. F., E. Bucsela, E. Brinksma, and J. F. Gleason (2002), NO_2, in *OMI Algorithm Theoretical Basis Document, Volume IV: Trace Gas Algorithms*, edited by K. Chance, KNMI, NASA/GSFC, FMI, pp. 15–36.

Boersma, K. F., H. J. Eskes, and E. J. Brinksma (2004), Error analysis for tropospheric NO_2 retrieval from space, *J. Geophys. Res.*, *109*, doi:10.1029/2003JD003962, D04 311.

Boersma, K. F., D. J. Jacob, E. J. Bucsela, A. E. Perring, R. Dirksen, R. J. van der A, R. M. Yantosca, R. J. Park, and R. C. Cohen (2007), Validation of OMI tropospheric NO_2 observations during INTEX-B and application to constrain NOx emissions over the eastern United States and Mexico, *J. Geophys. Res.*, —, doi:---, —.

Bovensmann, H., J. P. Burrows, M. Buchwitz, J. Frerick, V. V. Rozanov, K. V. Chance, and A. P. H. Goede (1999), SCIAMACHY: Mission objectives and measurement modes, *J. Atmos. Sci.*, *56*, 127–150.

Brinksma, E. J., G. Pinardi, R. Braak, H. Volten, A. Richter, A. Schönhardt, M. van Roozendael, C. Fayt, C. Hermans, R. J. Dirksen, T. Vlemmix, A. J. C. Berkhout, D. P. J. Swart, H.Oetjen, F. Wittrock, T. Wagner, O. W. Ibrahim, G. de Leeuw, M. Moerman, R. L. Curier, E. A. Celarier, W. H. Knap, J. P. Veefkind, H. J. Eskes, M. Allaart, R. Rothe, A. J. M. Piters, and P. F. Levelt (2007), The 2005 and 2006 DANDELIONS NO_2 and aerosol validation campaigns, *J. Geophys. Res.*, —, —.

Bucsela, E., A. E. Perring, R. C. Cohen, J. F. Gleason, K. F. Boersma, M. O. Wenig, T. H. Bertram, P. J. Wooldrige, R. Dirksen, E. A. Celarier, and J. Veefkind (2007), A comparison of NO_2 *in situ* aircraft measurements with data from the Ozone Monitoring Instrument, *J. Geophys. Res.*, —, doi:---, —.

Bucsela, E. J., E. A. Celarier, M. O. Wenig, J. F. Gleason, J. P. Veefkind, K. F. Booersma, and E. J. Brinksma (2006), Algorithm for NO_2 vertical column retrieval from the Ozone Monitoring Instrument, *IEEE Trans. Geosci. Rem. Sens.*, *44*(5), doi:10.1109/TGRS.2005.863715, 1245–1258.

Burrows, J. P., A. Richter, A. Dehn, B. Deters, S. Himmelmann, S. Voigt, and J. Orphal (1999a), Atmospheric remote sensing reference data from GOME-2. temperature-dependent absorption cross-sections of O_3 in the 231-794 nm range, *J. Quant. Spectrosc. Radiat. Transfer*, *61*, 509517.

Burrows, J. P., M. Weber, M. Buchwitz, V. V. Rozanov, A. Ladstatter-Weissenmayer, A. Richter, R. DeBeek, R. Hoogen, K. Bramstedt, and K. U. Eichmann (1999b), The global ozone monitoring experiment (GOME): Mission concept and first scientific results, *J. Atmos. Sci.*, *56*, 151–175.

Cageao, R. P., J. F. Blavier, J. P. McGuire, Y. B. Jiang, V. Nemtchinov, F. P. Mills, and S. P. Sander (2001), High resolution fourier transform ultraviolet-visible spectrometer for the measurement of atmospheric trace species: Application to OH, *Appl. Opt.*, *40*, 2024–2030.

Cede, A., J. Herman, R. Richter, N. Krotkov, and J. Burrows (2006), Measurements of nitrogen dioxide total column amounts using a brewer double spectrophotometer in direct sun mode, *J. Geophys. Res.*, *111*, doi:10.1029/2005JD006585.

Celarier, E. A., J. F. Gleason, E. J. Bucsela, K. F. Boersma, E. Brinksma, J. P. Veefkind, and P. Levelt (2006), OMNO2 README file, Tech. rep., NASA Goddard Space Flight Center. URL `http://toms.gsfc.nasa.gov/omi/no2/OMNO2_readme.pdf`.

Chance, K. V. and R. J. D. Spurr (1997), Ring effect studies: Rayleigh scattering, including molecular parameters for rotational Raman scattering, and the Fraunhofer spectrum, *Appl. Opt.*, *36*(21), 5224–5230.

Cleary, P. A., P. J. Wooldridge, and R. C. Cohen (2002), Laser-induced fluorescence detection of atmospheric NO_2 with a commercial diode laser and a supersonic expansion, *Appl. Opt.*, *41*, 6950–6956.

Denis, L. e. a. (2005), A new software suite for NO_2 vertical profile retrieval from ground-based zenith-sky spectrometers, *J. Quant. Spectrosc. Radiat. Transfer*, *92*(3), 321–333.

Deutschmann, T. and T. Wagner (2006), *TRACY-II Users manual*, University of Heidelberg.

Dobber, M., R. Dirksen, P. Levelt, G. van den Oord, R. Voors, Q. Kleipool, G. Jaross, M. Kowalewski, E. Hilsenrath, G. Leppelmeier, J. de Vries, W. Dierssen, and N. Rozemeijer (2006), Ozone monitoring instrument calibration, *IEEE Trans. Geosci. Rem. Sens.*, *44*(5), doi:10.1109/TGRS.2006.869987, 1209–1238.

Finlayson-Pitts, B. J. and J. Pitts, James N. (2000), *Chemistry of the Upper and Lower Atmosphere: Theory, Experiments, and Applications*, Academic Press, ISBN 012-257060X.

Gordley, L., J. Russell, L. Mickley, J. Frederick, J. Park, K. Stone, G. Beaver, J. McInerney, L. Deaver, G. Toon, F. Murcray, R. Blatherwick, M. Gunson, J. Abbatt, R. Mauldin, G. Mount, B. Sen, and J. Blavier (1996), Validation of nitric oxide and nitrogen dioxide measurements made by the halogen occultation experiment for UARS platform, *J. Geophys. Res.*, *101*(D6), doi:A1996UJ40400034, 10 241–10 266.

Heland, J., H. Schlager, A. Richter, and J. P. Burrows (2002), First comparison of tropospheric NO_2 column densities retrieved from GOME measurements and in situ aircraft profile measurements, *Geophys. Res. Lett.*, *29*(20), Article No. 1983.

Ionov, D., F. Goutail, and J. Pommereau (2006a), Validation of satellite data on total NO_2: GOME, SCIAMACHY and OMI nadir viewing instruments compared to UV-visible SAOZ network, in *Proc. of 3rd International DOAS Workshop, Bremen, 20-22 March, 2006*, pp. —.

Ionov, D., F. Goutail, J.-P. Pommereau, A. Bazureau, E. Kyro, T. Portafaix, G. Held, P. Ericksen, and V. Dorokhov (2006b), Ten years of NO_2 comparisons between ground-based SAOZ and satellite instruments (GOME, SCIAMACHY, OMI), in *Atmospheric Science Conference, ESRIN, Frascati, Italy, 8-12 May 2006*, ESA SP-628, pp. —.

Ionov, D., Y. Timofeyev, F. Goutail, J.-P. Pommereau, and A. Shalamyansky (2007), Delta-validation of ENVISAT SCIAMACHY total ozone and NO_2 with the data of ground-based UV-VIS measurements (m-124 and SAOZ), in *3rd Workshop on the Atmospheric Chemistry Validation of Envisat (ACVE-3), ESRIN, Italy, 4-7 December 2006*, ESA SP-642, pp. —.

Kurucz, R. L., I. Furenlid, J. Brault, and L. Testerman (1984), *Solar flux atlas from 296 nm to 1300 nm*, vol. National Solar Observatory Atlas No. 1, National Solar Observatory.

Lambert, J., M. Van Roozendael, P. Simon, J. Pommereau, F. Goutail, J. Gleason, S. Andersen, D. Arlander, N. Van, H. Claude, J. de la Noe, M. De Maziere, V. Dorokhov, P. Eriksen, A. Green, K. Tornkvist, B. Hoiskar, E. Kyro, J. Leveau, M. Merienne, G. Milinevsky, H. Roscoe, A. Sarkissian, J. Shanklin, J. Stahelin, C. Tellefsen, and G. Vaughan (2001), Combined characterisation of GOME and TOMS total ozone measurements from space using ground-based observations from the NDSC, *Adv. Space Res.*, *26*(12), 1931–1940.

Levelt, P. F. and P. K. Bhartia (2007), Tbd, *J. Geophys. Res.*, *TBD*(TBD), doi:TBD, TBD.

Levelt, P. F., E. Hilsenrath, G. W. Leppelmeier, G. H. J. van den Oord, P. K. Bhartia, J. Taminnen, J. F. de Haan, and J. P. Veefkind (2006a), Science objectives of the Ozone Monitoring Instrument, *IEEE Trans. Geosci. Rem. Sens.*, *44*(5), doi:10.1109/TGRS.2006.872336, 1199–1208.

Levelt, P. F., G. H. J. van den Oord, M. R. Dobber, A. Malkki, H. Visser, J. de Vries, P. Stammes, J. Lundell, and H. Saari (2006b), The Ozone Monitoring Instrument, *IEEE Trans. Geosci. Rem. Sens.*, *44*(5), doi:10.1109/TGRS.2006.872333, 1093–1101.

Martin, R., C. Sioris, K. Chance, T. Ryerson, T. Bertram, P. Woolridge, R. Cohen, J. Neuman, A. Swanson, and F. Flocke (2006), Evaluation of space-based constraints on nitrogen oxide emissions with regional aircraft measurements over and downwind of eastern north america, *J. Geophys. Res.*, *111*, doi:10.1029/2005JD006680.

Martin, R. V., D. J. Jacob, J. A. Logan, I. Bey, R. M. Yantosca, A. C. Staudt, Q. Li, A. M. Fiore, B. N. Duncan, H. Liu, P. Ginoux, and V. Thouret (2002), Interpretation of TOMS observations of tropical tropospheric ozone with a global model and in situ observations, *J. Geophys. Res.*, *107*(D18), Article No. 4351.

Nizkorodov, S. A., S. P. Sander, and L. R. Brown (2004), Temperature and pressure dependence of high-resolution air-broadened absorption cross sections of NO_2 (415–525 nm), *J. Phys. Chem.*, *A108*, 4864–4872.

Piters, A., K. Bramstedt, J. Lambert, and B. Kirchhoff (2006), Overview of sciamachy validation: 2002-2004, *Atmos. Chem. & Phys.*, *6*, 127–148.

Platt, U. (1994), *Chemical Analysis Series, 127, Differential optical absorption spectroscopy (DOAS), Air monitoring by spectroscopic techniques*, John Wiley & Sons, Inc.

Russchenberg, H., F. Bosveld, D. Swart, H. ten Brink, G. de Leeuw, R. Uijlenhoet, B. Arbesser-Rastburg, H. van der Marel, L. Ligthart, R. Boers, and A. Apituley (2005), Groundbased atmospheric remote sensing in The Netherlands; European outlook, *IEICE Transactions on Communications*, *E88-B(6)*, doi:10.1093/ietcom/e88-b.6.2252, 2252–2258.

Spurr, R. J. D. (2001), Linearized radiative transfer theory: A general discrete ordinate approach to the calculation of radiances and analytic weighting functions, with application to atmospheric remote sensing, Ph.D. thesis, Technical University of Eindhoven, The Netherlands.

Spurr, R. J. D., T. P. Kurosu, and K. V. Chance (2001), A linearized discrete ordinate radiative transfer model for atmospheric remote sensing retrieval, *J. Quant. Spectrosc. Radiat. Transfer*, *68*, 689–735.

Thornton, J. A., P. J. Wooldridge, and R. C. Cohen (2000), Atmospheric NO_2: In situ laser-induced fluorescence detection at parts per trillion mixing ratios, *Analytical Chemistry*, *72*, 528–539.

Vandaele, A. C., C. Hermans, P. C. Simon, M. Carleer, R. Colin, S. Fally, M. F. Mérienne, A. Jenouvrier, and B. Coquart (1998), Measurements of the NO_2 absorption cross-section from 42000 cm^{-1} to 10000 cm^{-1} (238–1000 nm) at 220 K and 294

K, *J. Quant. Spectrosc. Radiat. Transfer*, *59*, 171–184.

Veefkind, J. P. and E. A. Celarier (2006), OMI level 2 NO2 data product specification, Tech. Rep. SD-OMIE-KNMI-352, KNMI and NASA Goddard Space Flight Center. URL `http://disc.sci.gsfc.nasa.gov/Aura/OMI/OMNO2_data_product_specification.pdf`.

Veefkind, J. P., E. J. Brinksma, K. F. Boersma, H. Eskes, J. F. Gleason, E. J. Bucsela, E. A. Celarier, M. O. Wenig, and P. F. Levelt (2007), High spatial resolution NO_2 observations over europe using data from the ozone monitoring instrument, *Geophys. Res. Lett.* (To appear.).

Wagner, T., B. Dix, C. v. Friedeburg, U. Frieß, S. Sanghavi, R. Sinreich, and U. Platt (2004), MAX-DOAS O4 measurements - a new technique to derive information on atmospheric aerosols. (I) Principles and information content, *J. Geophys. Res.*, *109*, doi:10.1029/2004JD004904.

Wagner, T., J. Burrows, T. Deutschmann, B. Dix, F. Hendrick, C. von Friedeburg, U. Frieß, K. Heue, H. Irie, H. Iwabuchi, Y. Kanaya, J. Keller, C. A. McLinden, H. Oetjen, E. Palazzi, A. Petritoli, U. Platt, O. Postylyakov, J. Pukite, A. Richter, M. van Roozendael, A. Rozanov, V. Rozanov, R. Sinreich, S. Sanghavi, and F. Wittrock (2007), Comparison of Box-Air-Mass-Factors and Radiances for Multiple-Axis Differential Optical Absorption Spectroscopy (MAX-DOAS) Geometries calculated from different UV/visible Radiative Transfer Models, *Atm. Chem. Phys*, *accepted*.

Wenig, M. O., A. M. Cede, E. J. Bucsela, E. A. Celarier, K. F. Boersma, J. P. Veefkind, E. Brinksma, J. F. Gleason, and J. R. Herman (2007), Validation of omi tropospheric no_2 column densities using direct-sun mode brewer measurements at nasa goddard space flight center, *J. Geophys. Res.*, —, doi:---, —.

Wittrock, F., H. Oetjen, A. Richter, S. Fietkau, T. Medeke, A. Rozanov, and J. P. Burrows (2004), MAX-DOAS measurements of atmospheric trace gases in Ny-Ålesund - Radiative transfer studies and their application, *Atmos. Chem. Phys.*, *4*, 955–966.

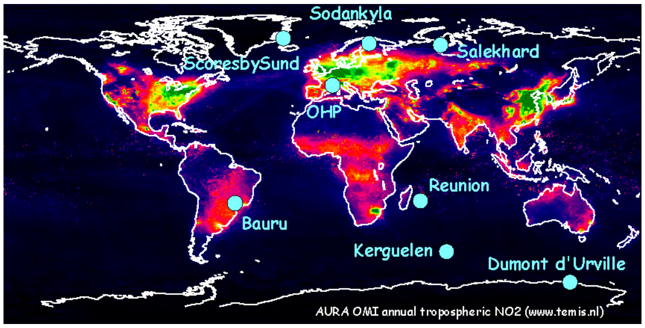

Figure 1. Geographical distribution of eight CNRS-operated SAOZ stations in the NDACC network. The colored field presented is the annual mean tropospheric NO_2 column amounts, as measured by OMI.

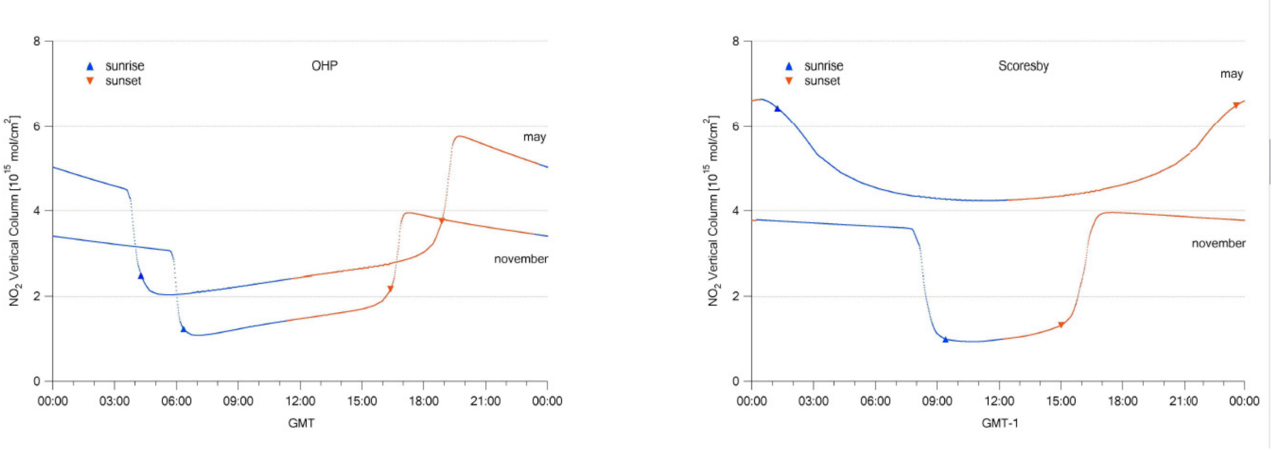

Figure 2. Simulated time-history of stratospheric NO_2 at a mid-latitude station (OHP), and a high-latitude station (Scoresbysund), for spring and fall.

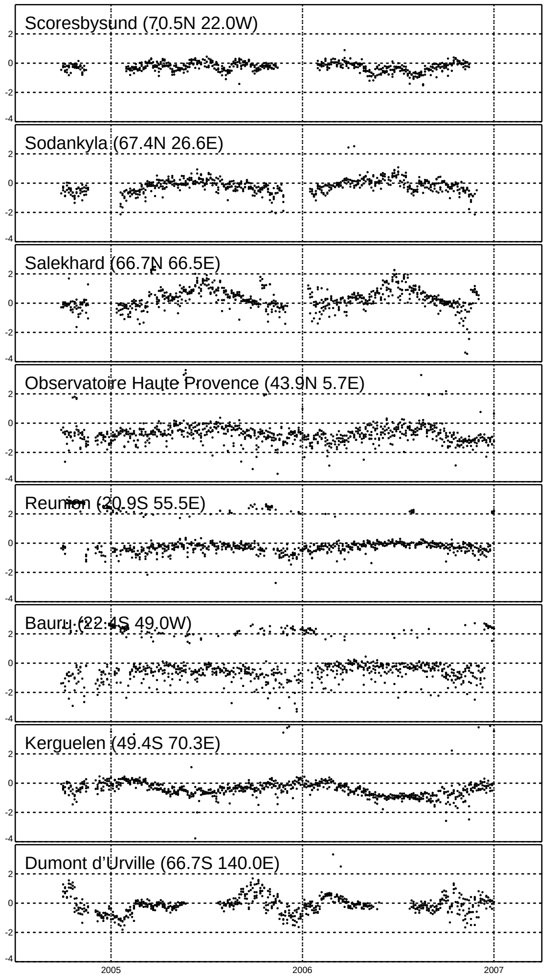

Figure 3. Time series of the difference between OMI and SAOZ-measured stratospheric NO_2 in units of $10^{15}\mathrm{cm}^{-2}$. The sites are ordered from North to South.

Table 1. Absolute average and r.m.s. difference (Δ, ρ; $\times 10^{15}$ cm^{-2}), and correlation (R) between ground-based SAOZ and satellite data, adjusted to sunrise OMI total and stratospheric NO_2 (2004-2006)

Station	OMI–SAOZ total column			OMI–SAOZ strat. column		
	Δ	ρ	R	Δ	ρ	R
Scoresby Sund	+0.02	0.82	0.93	−0.33	0.44	0.99
Sodankyla	+0.58	2.03	0.71	−0.28	0.56	0.97
Salekhard	+1.05	1.57	0.86	+0.24	0.73	0.95
OHP	+1.48	2.39	0.49	−0.71	0.90	0.74
Reunion	+0.17	0.73	0.31	−0.45	0.56	0.67
Bauru	+0.63	2.03	0.17	−0.80	0.97	0.58
Kerguelen	−0.04	0.58	0.88	−0.37	0.59	0.89
Dumont dUrville	+0.27	1.10	0.88	−0.23	0.66	0.96
OVERALL:	+0.53	1.56	0.70	−0.37	0.70	0.92

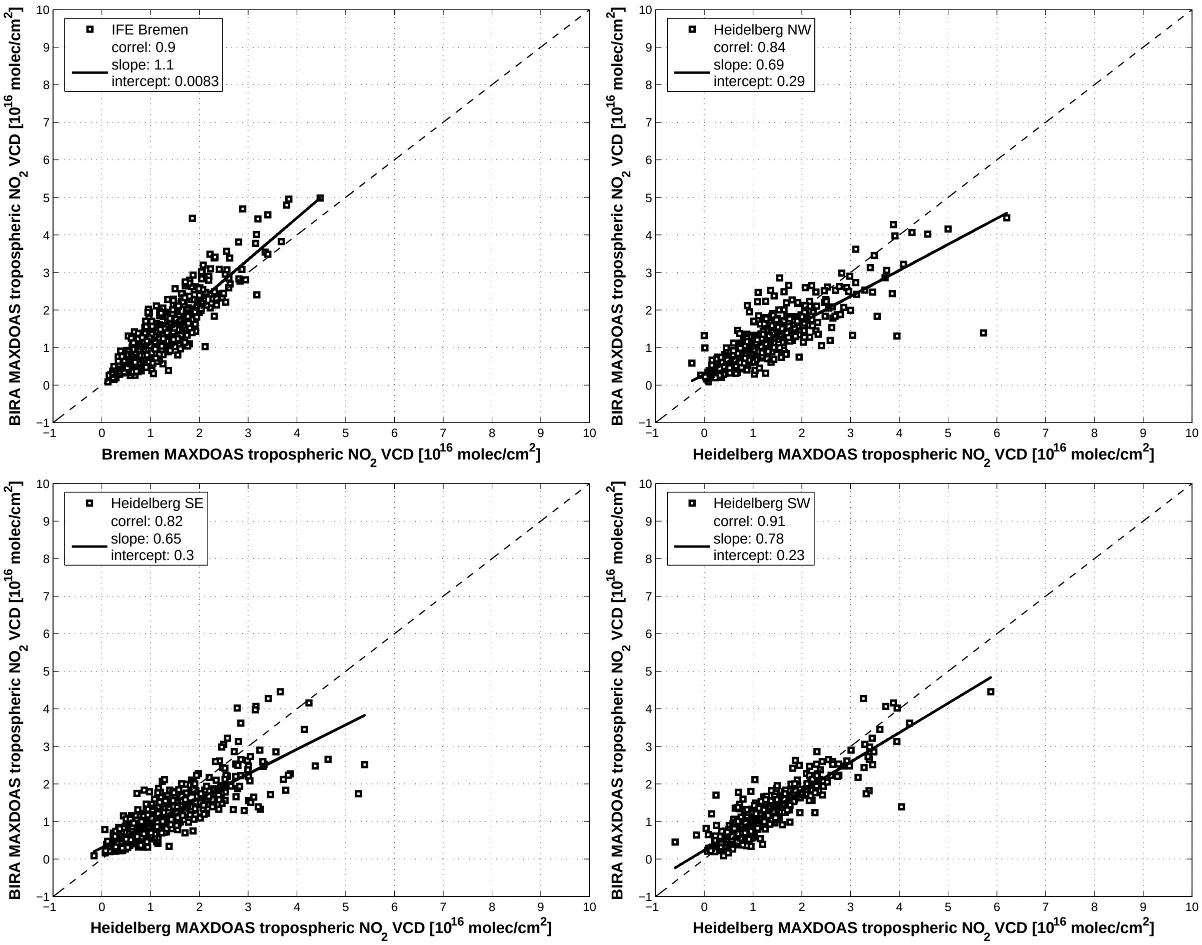

Figure 4. Scatter plots of the tropospheric NO_2 columns retrieved during the 2005 campaign from the BIRA MAX-DOAS instrument and, respectively, the Bremen MAX-DOAS (top left), the Heidelberg MAX-DOAS for the 3 pointing directions North-West (top right), South-East (bottom left) and South-West (bottom right). The regression analysis parameters are given in the legends. It has to be noted that agreement with the Heidelberg observations can be further improved after homogenisation of the retrieval settings (see text).

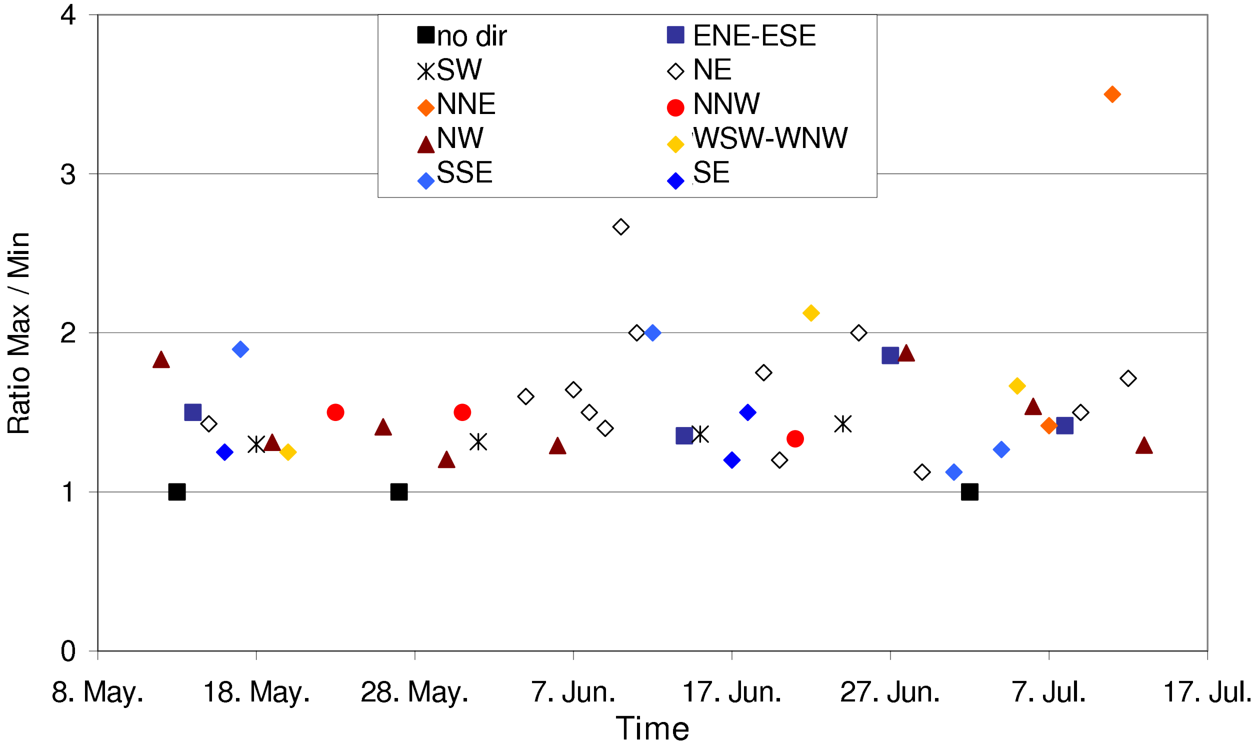

Figure 5. Maximum and minimum NO_2 SCD observed for an elevation angle of 3° of the Heidelberg MAX-DOAS telescopes observing under three different azimuth angles at Cabauw during the DANDELIONS campaign in 2005. High ratios indicate large horizontal gradients of the tropospheric NO_2 concentration field, colors indicate the direction of the gradient (directed toward higher values).

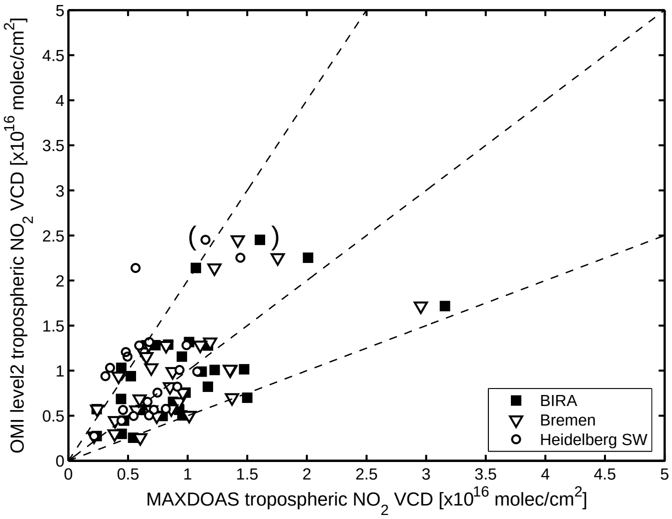

Figure 6. Correlations between tropospheric NO$_2$ from the three MAX-DOAS instruments at Cabauw (BIRA, Bremen, and Heidelberg SW direction) and OMI Level-2 OMI data are included if cloud fractions were less than 20%. Correlation and regression coefficients are summarized in Table 2. The dashed lines are provided as a visual aid, and show slopes of 1/2, 1, and 2. The data point in brackets is clearly an outlier (see text), and was not included in the regression analysis presented in table 2.

Table 2. Summary of statistical analyses of comparisons between tropospheric NO$_2$ from MAX-DOAS data and OMI Level-2.

	N	R	Intercept	Slope	RMS diff.	Relative RMS diff.
BIRA south	29	0.60	4.29	0.52	4.82	52%
Bremen southwest	29	0.63	3.93	0.59	4.44	48%
Heidelberg southwest	21	0.45	4.27	0.8	5.38	56%
Heidelberg spatial average	21	0.65	1.99	0.85	3.89	40%

N denotes number of collocations, and R is Pearson correlation coefficient. The intercept and (absolute) RMS difference are in units of $10^{15}\,\mathrm{m}^{-2}$

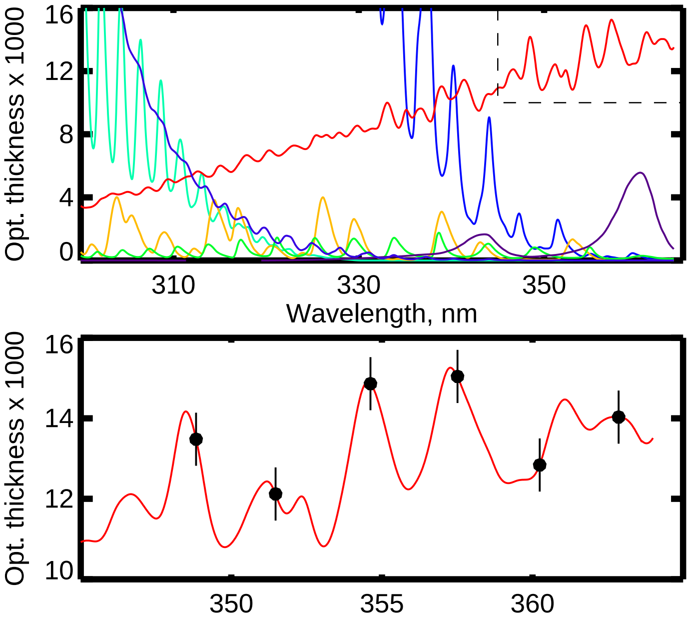

Figure 7. Typical optical depths of the main trace gases in the Brewer MK-III wavelength range. Lower: NO2 optical depth for 1 DU ($= 2.7 \times 10^{16}\,\mathrm{cm}^{-2}$), 6 slit positions with noise estimates.

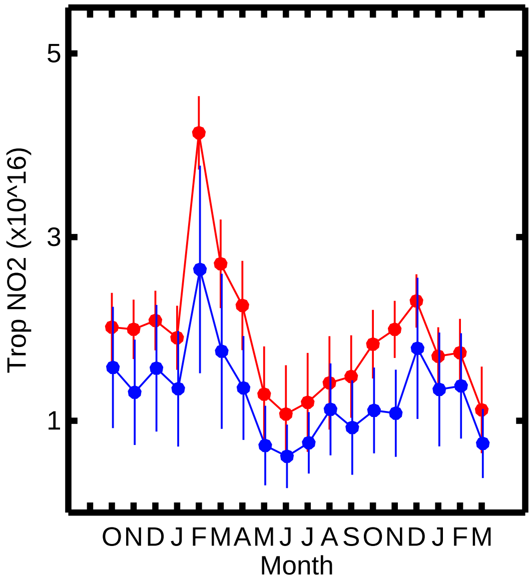

Figure 8. Comparison between the monthly mean Brewer-measured and OMI-measured NO_2 total columns.

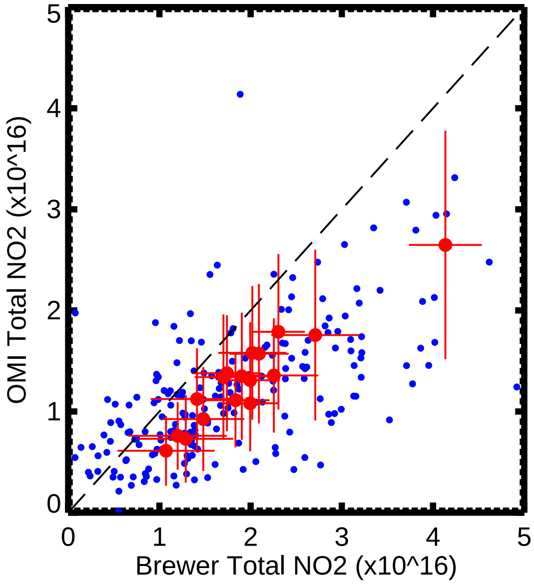

Figure 9. Daily mean and monthly mean values of NO_2 total column measured by the Brewer instrument and OMI. The line of linear regression is also shown.

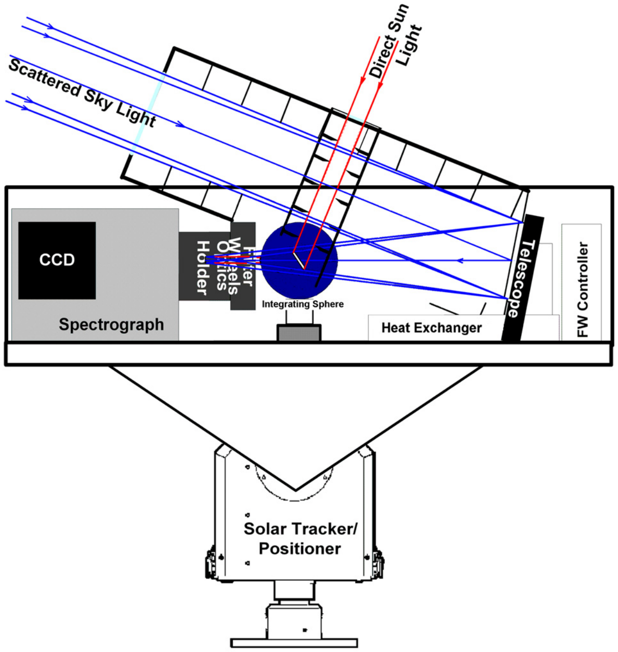

Figure 10. Schematic drawing of the MF-DOAS instrument.

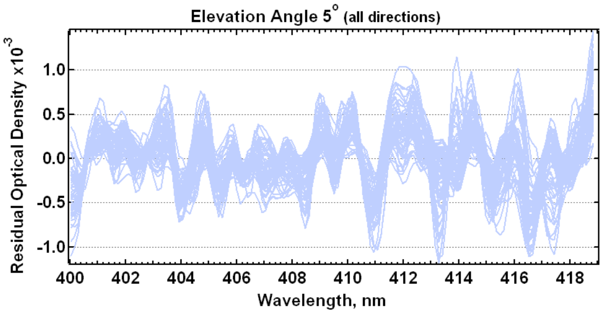

Figure 11. Representative residual optical densities for observations of May 9, 2006 at 5° elevation and 4 azimuth angles.

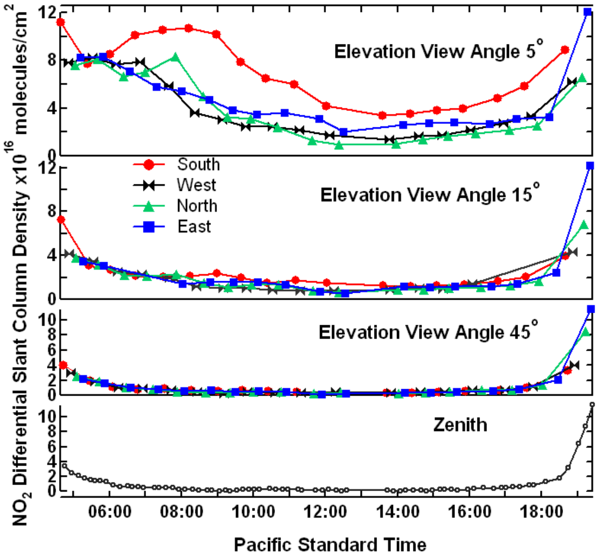

Figure 12. Example of measured spatial and temporal variation of MF-DOAS-measured NO_2 differential SCD for May 9, 2006

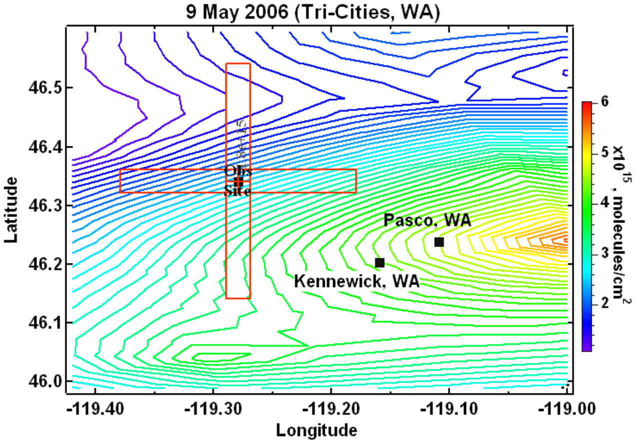

Figure 13. Tropospheric NO_2 VCD over the Tri-Cities area of Washington State on May 9, 2006. The contour map is derived from the individual OMI FOV measurements.

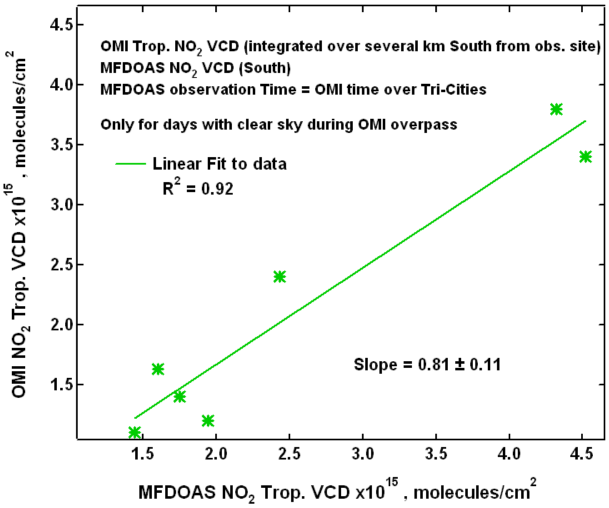

Figure 14. Correlation between OMI tropospheric NO_2 vertical column and MF-DOAS NO_2 tropospheric VCD for measurements made from April 30 through May 13, 2006

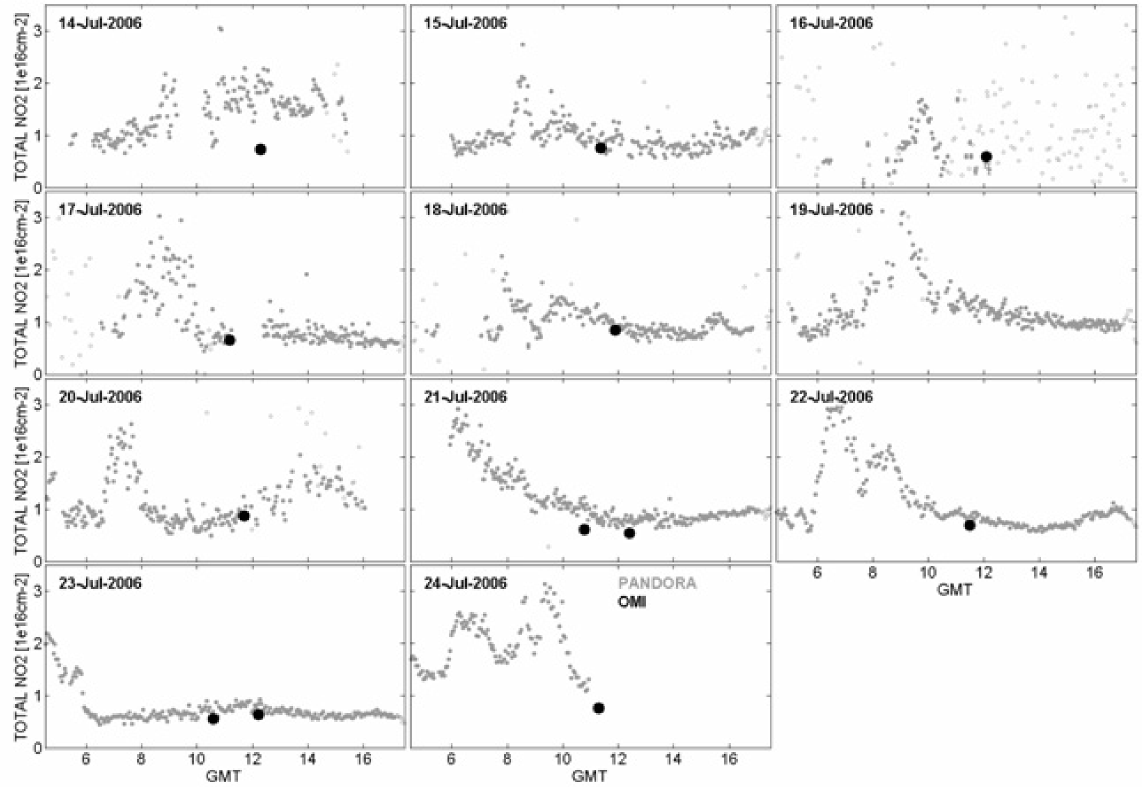

Figure 15. Pandora-1 Data measured during the period 14–24 July 2006, in Thessaloniki (grey dots) and OMI overpass data for the site (large black dots).

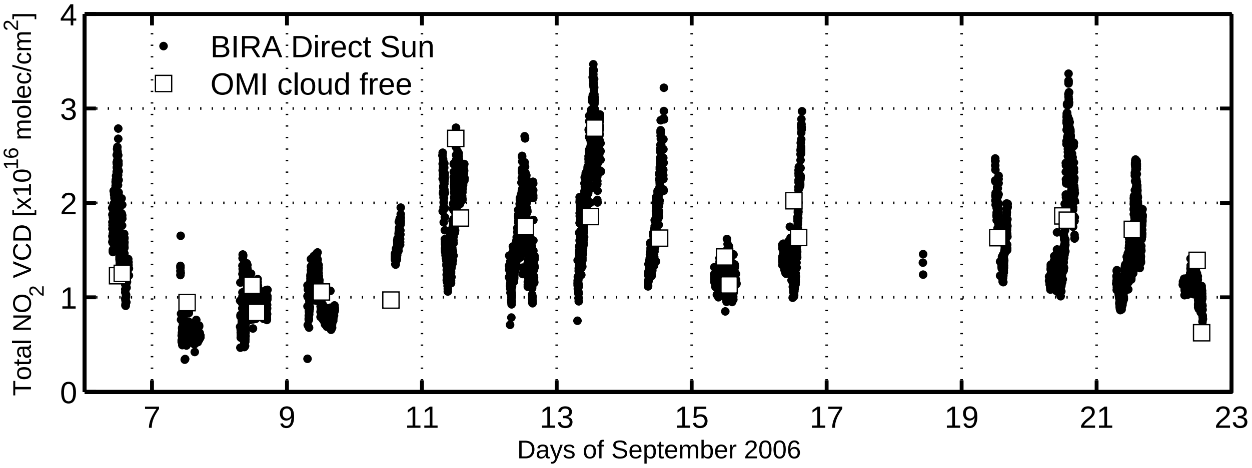

Figure 16. Time series of NO_2 VCD measured by the BIRA direct-sun DOAS instrument. The open squares show the collocated OMI measurements.

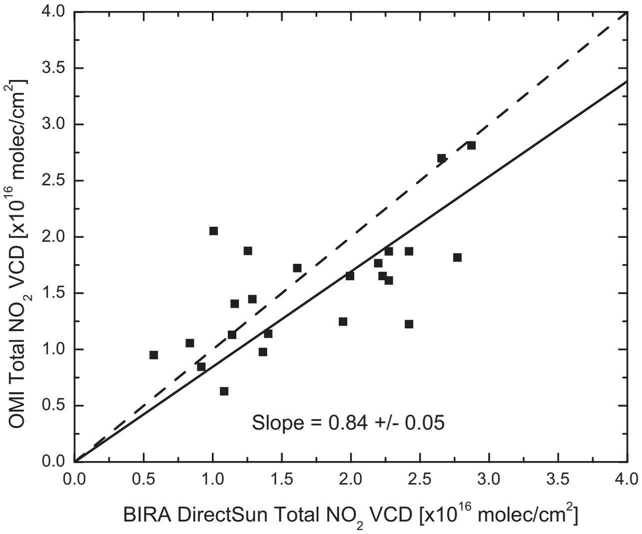

Figure 17. Correlation plot showing the collocated OMI and BIRA direct-sun DOAS instrument measurements (open squares in Figure 16).

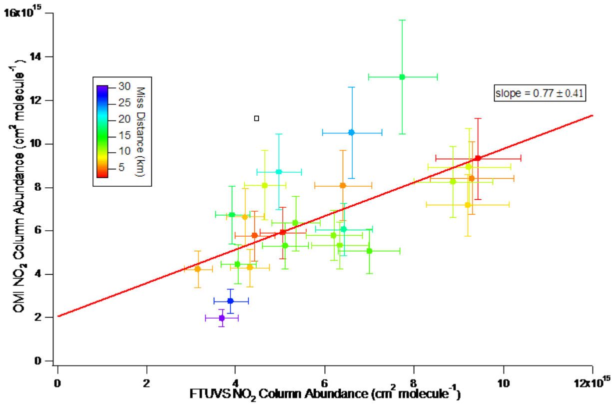

Figure 18. OMI versus FTUVS measurements of total column NO_2, binned by distance between TMF and the centroid of the OMI FOV (distance indicated by color, see inset scale)

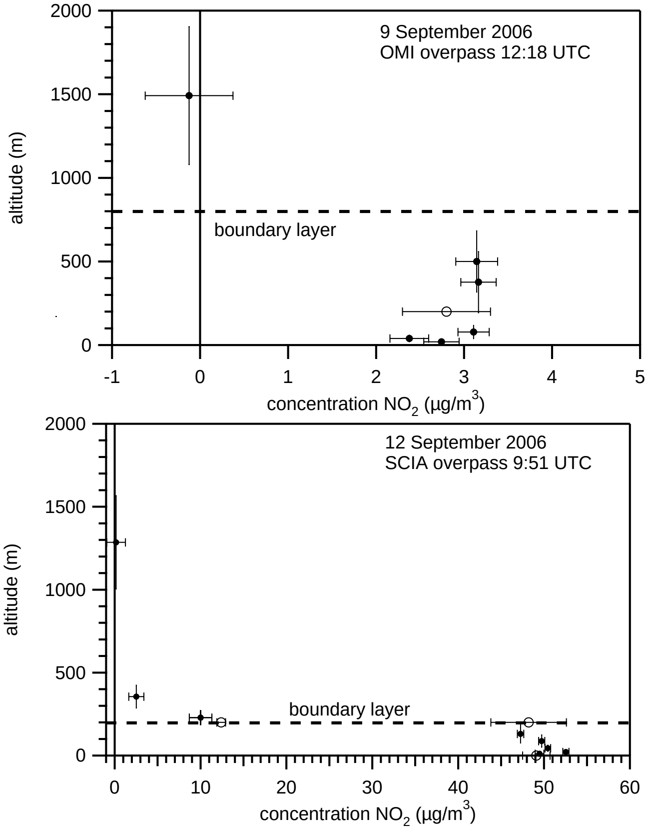

Figure 19. Lidar NO_2 profile (black circles) and NO_2 monitor value (open circle) measured at Cabauw. Horizontal bars indicate two-sigma values for the concentration. For the lidar data, vertical bars indicate the height intervals over which concentrations have been determined. The boundary layer height is indicated by a dashed line. Top panel: Clean day, September 9, 2006 (lidar measurement from 12:04–12:52 UT). On this day, the NO_2 monitor at ground level was not operational. NO_2 monitor data at 200 m were averaged over the lidar integration time. Bottom panel: Polluted day, September 12, 2006 (lidar measurement from 9:37–10:26 UT). For the NO_2 monitor data at ground level an average was made for the time the monitor was operational during this interval, from 10:03–10:17. For the data of the NO_2 monitor at 200 m two averages were determined; the lower average, for 9:37–10:17 UT, is for the situation that the NO_2 monitor is above the boundary layer, the higher value, for 10:16–10:26 UT, is for the situation that the NO_2 monitor is situated below the boundary layer.

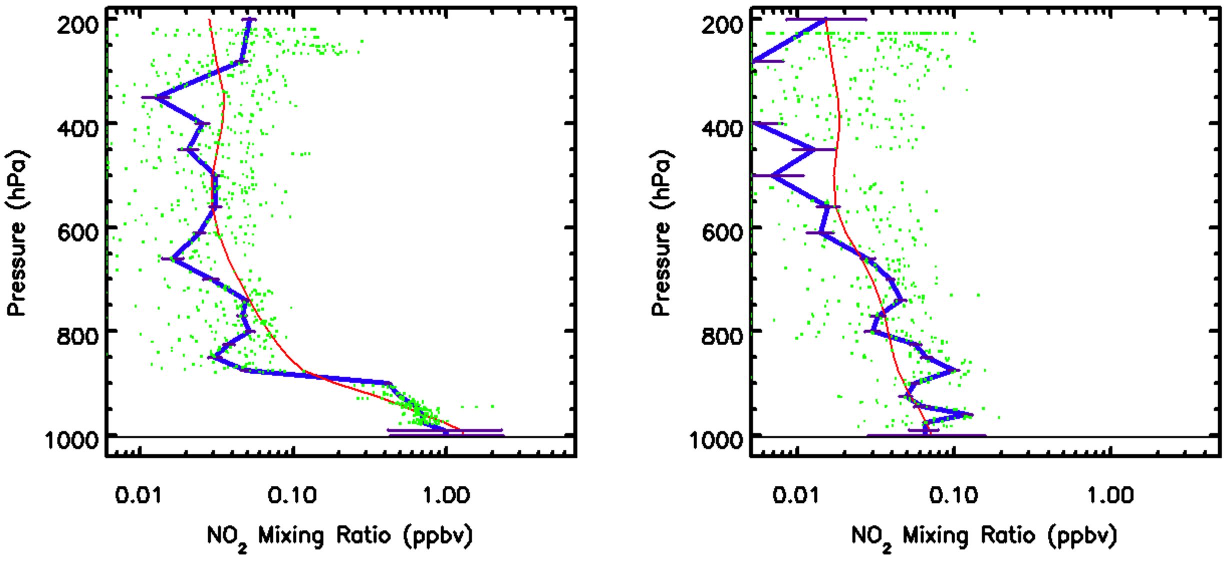

Figure 20. Two INTEX-B NO$_2$ profiles. The upper panel shows data for a profile measured over the Mississippi-Alabama border (32.0 N, 88.3 W), while the lower panel shows data for a profile measured over the Gulf of Mexico (23.0 N, 91.1 W). Green dots are original measurements, the blue line is binned profile, and the red line is the annual mean GEOS-CHEM model profile for that location.

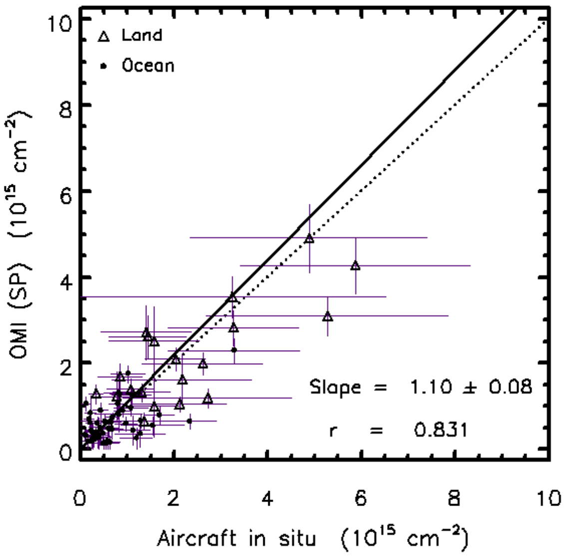

Figure 21. Tropospheric NO2 columns with *in situ* columns from INTEX-B. The symbols indicate land measurements (triangle) or ocean measurements (dot). The dotted line is a 1:1 ratio and the solid line is the fit to the data.

Table 3. Summary of validation study results for OMI NO_2 data product.

Instrument	Column	Group	OMI, rel. to GB	Remarks
SAOZ	Strat.	CNRS	+10%	As large as 50% in tropics.
MAX-DOAS	Trop.	BIRA, etc.	-15%	Large scatter in the data.
Brewer	Total	GSFC	-33%	Large N, large scatter.
MF-DOAS	Total	WSU	-19%	Very small N.
Pandora-1	Total	GSFC	-15%	Very small N.
DS-DOAS	Total	BIRA	-16%	Small N, large scatter.
FTUVS	Total	JPL	-23%	Small N, but good correlation.
Aircraft *in situ*	Trop.	UC Berkeley, GSFC	+10%	Large scatter.